

PROTEINS MOVE! PROTEIN DYNAMICS AND LONG-RANGE ALLOSTERY IN CELL SIGNALING

By ZIMEI BU* AND DAVID J. E. CALLAWAY*†

*Department of Chemistry, The City College of New York, New York, New York, USA

†New York University School of Medicine, New York, New York, USA

I.	Introduction	164
II.	NHERF1 Modulates the Macromolecular Assembly, Cell Surface Retention, and Subcellular Localization of Membrane Proteins.....	167
A.	CFTR	167
B.	NaPiT2a	168
C.	Podocalyxin Complexes	169
D.	Tyrosine Kinase Receptor Complexes	170
III.	Signal Transduction by Allosteric Scaffolding Protein Interactions.....	171
A.	Allosteric Modulation of NHERF1 to Assemble Membrane Complexes....	173
B.	Negative Cooperativity and Feedback Loop	174
IV.	Structural Basis of Autoinhibition and Long-Range Allostery in NHERF1	178
A.	NHERF1 Has a Highly Elongated Shape, Allowing Long-Range Interdomain Allosteric Communications.....	179
B.	Allosteric Control in NHERF1 Originates from Domain–Domain Interactions.....	181
C.	Redefinition of the Structural Boundary of PDZ Domains	183
D.	Autoinhibition of PDZ2 by the C-Terminal Domain of NHERF1.....	185
E.	Disease-Associated NHERF1 Mutations Affect the Structure, Stability, and Binding Capability of PDZ Domains	185
V.	Dynamic Propagation of Allosteric Signals by Nanoscale Protein Motion	186
A.	The Physical Concepts Behind Protein Dynamics.....	187
B.	Nanoscale Protein Dynamics: The Emergence of a New Frontier	189
C.	Dynamic Propagation of Allosteric Signals by Nanoscale Protein Motion...	202
D.	A Simple Four-Point Model Describes Domain Motion	207
E.	The Importance of NSE and a Plan for the Future	211
VI.	Summary and Perspective	213
	References.....	214

ABSTRACT

An emerging point of view in protein chemistry is that proteins are not the static objects that are displayed in textbooks but are instead dynamic actors. Protein dynamics plays a fundamental role in many diseases, and spans a large hierarchy of timescales, from picoseconds to milliseconds or

even longer. Nanoscale protein domain motion on length scales comparable to protein dimensions is key to understanding how signals are relayed through multiple protein–protein interactions. A canonical example is how the scaffolding proteins NHERF1 and ezrin work in coordination to assemble crucial membrane complexes. As membrane–cytoskeleton scaffolding proteins, these provide excellent prototypes for understanding how regulatory signals are relayed through protein–protein interactions between the membrane and the cytoskeleton. Here, we review recent progress in understanding the structure and dynamics of the interaction. We describe recent novel applications of neutron spin echo spectroscopy to reveal the dynamic propagation of allosteric signals by nanoscale protein motion, and present a guide to the future study of dynamics and its application to the cure of disease.

I. INTRODUCTION

Proteins move! This simple statement encapsulates a wide variety of phenomena that are central for the understanding of life and for the cure of disease. Proteins are composed of multiple domains, whose flexibility and mobility lead to a great deal of versatility in their function. Protein dynamics (particularly at the domain level) is a controlling influence in the allosteric formation of protein complexes, in catalysis, in cell signaling and regulation, in metabolic transport, and in cellular locomotion. Yet, despite the importance of protein domain dynamics, the study of this field is in its infancy, largely because of the paucity of biophysical methods that are able to probe this regime. We here provide a review of some of the field, and propose a roadmap for future exploration. In order to understand what is known about protein dynamics and the significance of the challenges ahead, it is essential to review some of the relevant concepts. In order to motivate this discussion, we will first present a review of the biological relevance of long-range allosteric effects that couple the dynamics of protein domains.

In cells, membrane channels and receptors are often assembled into macromolecular complexes in specialized subcellular domains for the dynamic control of diverse cellular events. For instance, forming “quaternary” complexes of receptors, such as the EGF receptor or the PDGF receptor is necessary for initializing cascades of signaling events for cell growth and proliferation (Schlessinger, 1988). The function of ion

transport proteins, such as the cystic fibrosis transmembrane conductance regulator (CFTR) or sodium–phosphate cotransporter 2a (NaPiT2a), is regulated by a network of interactions with other membrane proteins, such as the G-protein coupled receptors and other ion channels by forming membrane oligomers either directly, or via cytosolic proteins as adapters or scaffolds. Forming large adherence membrane complexes at the cell–cell junctions is essential to maintain tissue integrity and to suppress tumor cell invasion (Yap et al., 1997; Perez-Moreno et al., 2003; Pujuguet et al., 2003). Understanding how transmembrane protein complexes are regulated and disregulated in disease state can help to identify elements as target to treat various diseases.

The mammalian Na^+/H^+ exchange regulatory factor (NHERF) family proteins are scaffolding proteins that assemble macromolecular complexes of transmembrane proteins, and regulate receptor signaling and ion transport (Shenolikar et al., 2004; Lamprecht and Seidler, 2006; Weinman et al., 2006). Members of this protein family, which contain two or more copies of modular PDZ (PSD-95/Discs-large/ZO-1) domains (Fig. 1), localize in the apical membrane region of polarized epithelial cells (Donowitz et al., 2005; Thelin et al., 2005). The PDZ domains are protein–protein interaction modules that are capable of binding to specific PDZ-binding motifs residing in the cytoplasmic portion of a large number of transmembrane proteins (Harris and Lim, 2001). Scaffolding proteins containing multiple PDZ domains and/or other protein–protein interaction modular domains can assemble membrane complexes as well as bring the membrane complexes into proximity with other cytosolic signaling molecules to assemble highly regulated signaling complexes (Sheng and Sala, 2001).

As the first member of the NHERF family, NHERF1 consists of two PDZ domains, PDZ1 and PDZ2 that bind to membrane proteins. NHERF1 also contains carboxy-terminal domain that binds to the membrane–cytoskeleton linker protein ezrin (EB) (Reczek and Bretscher, 1998) (Fig. 1). NHERF1 was shown to interact with ezrin, and therefore is also called ezrin-binding protein 50 or EBP50 (Reczek et al., 1997). The PDZ domains of NHERF1 interact with a number of transmembrane proteins. Some of the NHERF target proteins are implicated in human diseases (Takahashi et al., 2006; Kwon et al., 2007; Sizemore et al., 2007). The well-known functions of NHERF1 include assembling signaling complexes and regulating the endocytic recycling of the CFTR, cell surface adhesion and

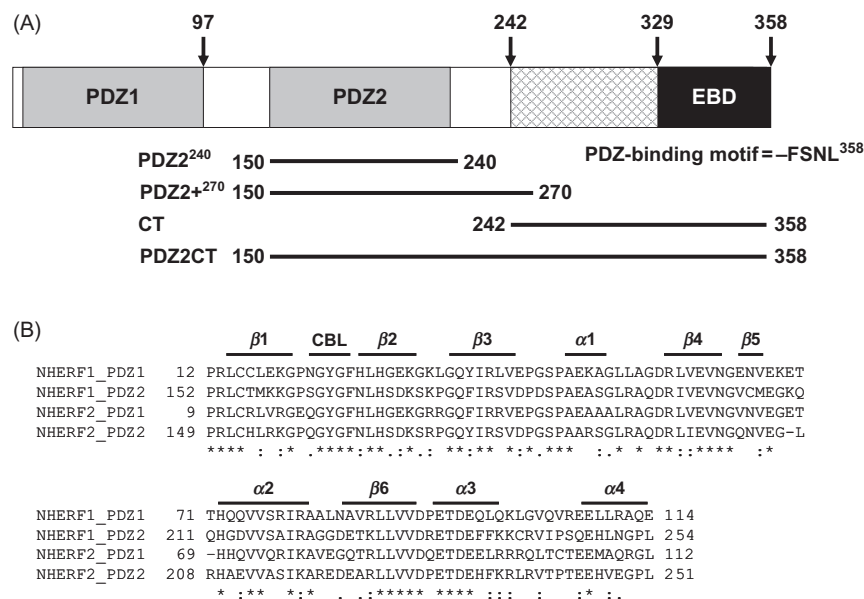


FIG. 1. (A) Schematic representation of the domain structure of human NHERF1. The carboxy-terminal end of the EB domain contains a canonical PDZ-binding motif. The amino acid positions of the differently truncated domains, including the putative PDZ2²⁴⁰ and that of PDZ2+²⁷⁰ with the extra carboxy-terminal helical subdomain, are shown. (B) Sequence alignment of the PDZ domains of human NHERF1 and NHERF2 proteins, annotated with secondary structure elements (CBL, carboxylate-binding loop). The residues involved in ligand binding are shown in bold. The alignment indicates that the sequence in the extra subdomain formed by $\alpha 3$ and $\alpha 4$ is conserved.

antiadhesion proteins such as podocalyxin, G-protein coupled receptors, and tyrosine kinase receptors PDGFR and EGFR (Hall et al., 1998a; Cao et al., 1999; Ko et al., 2004; Schmieder et al., 2004; Weinman et al., 2006). NHERF1 mutations, which affect its ability to assemble the transmembrane NaPiT2a, are correlated with impaired renal phosphate reabsorption in patients with chronic kidney disease (Karim et al., 2008). Altered subcellular localization of NHERF1 is associated with breast cancer progression (Mangia et al., 2009).

The function of NHERF1 and the interactions of NHERF1 with membrane transport proteins and receptors have been reviewed earlier (Shenolikar et al., 2004; Weinman et al., 2006). Recent progress in

understanding the structure and function of ezrin and other *ezrin-moe-sin-radixin* (ERM) proteins has been reviewed (Bretscher et al., 2002; Fievet et al., 2007; McClatchey and Fehon, 2009; Fehon et al., 2010). Here, we first summarize several representative cases that identify NHERF1 as an important factor to assemble complexes of transmembrane receptors or transport proteins. We review the findings that the assembling of signaling complexes by NHERF1 is allosterically regulated. These biochemical studies illustrate that scaffolding or adapter proteins not only function as scaffolds to dock signaling partners but are also regulated transistors and switches that control the effective propagation of signals from a remote site to a specific location over a long distance. We then review the studies that aimed at understanding the structural and dynamic mechanisms of NHERF1 and its interactions with the membrane-cytoskeleton linker protein ezrin in the allosteric regulation of the assembly of membrane complexes. We show that the long-range allosteric-binding behavior is communicated through interdomain conformational and dynamic changes (Li et al., 2009; Bhattacharya et al., 2010; Farago et al., 2010). A recent study using a novel neutron spin echo (NSE) spectroscopy reveals the activation of long-range interdomain motions in NHERF1 on nanometer length scales and on submicrosecond timescale upon binding to ezrin (Farago et al., 2010). Protein domain motion on these timescales and on length scales comparable to protein dimensions can thus propagate allosteric binding signals dynamically. The long-range conformational changes and nanoscale dynamics during the interactions of NHERF1 and ezrin provide a paradigm for studying how cellular signals are transmitted allosterically over a long distance in the cellular signaling network.

II. NHERF1 MODULATES THE MACROMOLECULAR ASSEMBLY, CELL SURFACE RETENTION, AND SUBCELLULAR LOCALIZATION OF MEMBRANE PROTEINS

A. *CFTR*

The PDZ domains of NHERF1 interact with the C-terminal tail of CFTR (Hall et al., 1998a). Interaction of NHERF1 with CFTR increases the polarized expression of CFTR in the apical plasma membrane, as well as enhances the vectorial transport of chloride ions (Moyer et al., 2000;

Raghuram et al., 2001). Moreover, NHERF1 overexpression increases the cell surface expression of a disease-causing mutant of CFTR with a deletion at amino acid Phe508 (Δ F508) (Guerra et al., 2005; Bossard et al., 2007; Favia et al., 2009). The Δ F508 mutant, responsible for 80% of the cases of the genetic disease cystic fibrosis, is trapped in the endoplasmic reticulum after biosynthesis and fails to reach the cell membrane to perform its normal functions as a chloride ion channel. NHERF1 interacts with both CFTR and the G-protein coupled beta 2 adrenergic receptor (β_2 -AR), and assembles a signaling complex comprised of CFTR and β_2 -AR (Naren et al., 2003). This complex mediates the stimulation of the CFTR ion channel by the β_2 -AR receptor (Taouil et al., 2003; Singh et al., 2009).

Using fluorescence photobleaching recovery and single particle tracking, the effects of NHERF1 on the lateral mobility of CFTR in living cells (Haggie et al., 2004, 2006; Bates et al., 2006). CFTR has a significant immobile population (50%), but adding 10 histidine residues at the C-terminus of CFTR to mask the PDZ-binding motif abolished its association with NHERF1, reduced the immobile fraction, and increased mobility. The effects of CFTR interactions with the F-actin cytoskeleton via NHERF1 and ezrin were studied previously with similar methods with N-terminal GFP tag (Haggie et al., 2006). Although the immobile population of CFTR with N-terminal GFP tag is significantly smaller than that measured by Bates et al., the GFP labeled CFTR became mobile after truncation or blocking of the C-terminal PDZ-binding motif, disrupting CFTR association with actin by expressing a mutant NHERF1 lacking the ezrin-binding domain (EBD), or disrupting the F-actin cytoskeleton by latrunculin. The association of the CFTR C-terminus with NHERF1 and ezrin has been proposed to physically tether CFTR to the actin cytoskeleton (Short et al., 1998). Together these studies suggest that NHERF1 and ezrin function as adapters between CFTR and the F-actin cytoskeletal network to stabilize CFTR at the cell membrane and impedes endocytosis retrieval.

B. *NaPiT2a*

NHERF1 regulates the reabsorption of phosphate ions in the kidney (Hernando et al., 2002). In the proximal tubule of kidneys, the transmembrane transporter NaPiT2a is responsible for the reabsorption of phosphate from urine. Impaired renal phosphate reabsorption leads to kidney stone formation and bone demineralization. The ability of NaPiT2a to transport

phosphate ions depends on the correct localization of NaPiT2a at the apical membrane of polarized epithelial cells, which is modulated by the parathyroid hormone (PTH). PTH binding to receptor PTH1R triggers a cascade of cellular signaling events, including the activation of protein kinase C, which regulates NaPiT2a endocytosis and thus the capacity of NaPiT2a to uptake phosphate. NHERF1 interacts with both NaPiT2a and PTH1R by binding to the PDZ motifs in their respective cytoplasmic tails (Gisler et al., 2001; Mahon et al., 2002). However, it is not clear if NHERF1 assembles NaPiT2a and PTH1R into the same complex. NHERF1 is required for correct apical localization of NaPiT2a (Hernando et al., 2002). Ezrin and NHERF1 assemble the PTH1R and NPT2a complexes localized in the actin-containing microvilli in the apical domains of these cells. Upon PTH treatment, the PTH1R, NaPiT2a, NHERF1, and ezrin colocalize to endocytic vesicles and NaPiT2a-dependent phosphate uptake is markedly inhibited (Mahon, 2008).

A recent study correlates NHERF1 mutations with impaired renal phosphate reabsorption in patients (Karim et al., 2008). This study finds that three NHERF1 mutations, L110V, R153Q, and E225K are found in patients of chronic kidney disease with impaired renal phosphate reabsorption (Karim et al., 2008). The disease mutations of NHERF1, L110V, R153Q, and E225K inhibit phosphate transport by NPT2a, in a similar fashion as in NHERF1^{-/-} kidney cells (Cunningham et al., 2005).

C. Podocalyxin Complexes

The cell surface antiadhesion molecule podocalyxin is connected to the F-actin cytoskeleton via NHERF1 or NHERF2 and ezrin (Takeda et al., 2001; Schmieder et al., 2004). Podocalyxin is the main molecular component of the apical plasma membrane of podocyte foot processes (Kerjaschki et al., 1984). Disruption of the interactions of podocalyxin/NHERF/actin cytoskeleton results in loss of glomerular foot processes and the glomerular disease proteinuria in animal models (Takeda et al., 2001). Podocalyxin activates *RhoA* through NHERF and ezrin, leading to redistribution of actin filaments (Schmieder et al., 2004). Moreover, podocalyxin contributes to the progression of breast cancer by perturbing tumor cell adhesion (Somasiri et al., 2004). The interaction of podocalyxin with NHERF1 and/or ezrin increases the aggressiveness of breast and prostate cancer cells (Sizemore et al., 2007).

D. Tyrosine Kinase Receptor Complexes

NHERF1 interacts with a number of important cell surface receptors and organizes multiple signal transduction pathways between cell membranes and the cytoskeletal network. NHERF1 interacts with cell growth factor tyrosine kinase receptors such as the platelet-derived growth factor receptor (PDGFR; Maudsley et al., 2000) and the epidermal growth factor receptor (Lazar et al., 2004), and several G protein-coupled receptors that include the β_2 -AR (Hall et al., 1998b), the parathyroid hormone receptor (PTH1R) (Mahon and Segre, 2004), and the kappa-opioid receptor (Liu-Chen, 2004). NHERF1 and ezrin are responsible for organizing the trafficking, localization, and membrane targeting of these receptors (Hall et al., 1998b; Maudsley et al., 2000; Mahon et al., 2002; Sneddon et al., 2003). NHERF1 and ezrin work together to link PDGFR to the actin cytoskeletal network, and are responsible for transmitting signals from PDGFR to the cytoskeletal networks so as to influence a cell's ability to spread and to migrate (James et al., 2004).

The PDZ1 domain of NHERF interacts with an internal peptide motif located within the C-terminal regulatory domain of EGFR (Lazar et al., 2004). This interaction slows the rate of EGF-induced receptor degradation, and stabilizes EGFR at the cell surface. Recent evidence shows that increased cytoplasmic expression of NHERF1 is correlated with tumor progresses in breast cancer (Mangia et al., 2009). In metastatic breast tumors, the localization of NHERF1 is mainly cytoplasmic. This same study finds that NHERF1 colocalizes with the oncogenic receptor HER2/neu in invasive breast cancer cells, although it is not known if NHERF1 directly binds to the cytoplasmic domain of HER2/neu directly or through other proteins. Because NHERF1 and ezrin can anchor the receptors to F-actin, they could play the dual roles of forming transient receptor dimers and localizing the receptors in the right location in response to stimulation. Besides ligand-induced dimerization of the receptors, preformed receptor dimers are thought to be primed for ligand binding and signaling and may enable cells to respond in a polarized fashion to growth factor stimulation (Chung et al., 2010), especially during cell migration when a cell's leading edge is typically enriched in actin filaments.

III. SIGNAL TRANSDUCTION BY ALLOSTERIC SCAFFOLDING PROTEIN INTERACTIONS

The important feature of NHERF1 is its binding to ezrin and other members of the ERM proteins. The interaction of NHERF1 with F-actin is due to the NHERF1 C-terminal EBD (Reczek and Bretscher, 1998). Ezrin and other ERM proteins are the membrane–cytoskeleton adapter or scaffolding proteins that link cell membrane to the F-actin cytoskeleton. The ERM proteins contain an N-terminal FERM (4.1 *ezrin–radixin–moesin*) domain of about 300 amino acid residues, and a C-terminal actin-binding domain that is connected to the FERM domain by a coiled-coil helical domain (Gary and Bretscher, 1995; Li et al., 2007b).

In the dormant form, ezrin and other ERM proteins are negatively regulated by head-to-tail intramolecular interactions between the FERM domain and the C-terminal domain, reviewed in Fehon et al. (2010). Although the activation mechanisms are not fully understood, ezrin and other ERM proteins become activated when the autoinhibition interactions are thought to be disrupted upon phosphorylation and/or phospholipid PIP₂ binding (Matsui et al., 1999; Fievet et al., 2004; Roch et al., 2010). The activated ERM proteins are proposed to undergo large conformational changes (Matsui et al., 1998; Bretscher et al., 2000; Yonemura et al., 2002). The unmasked FERM domain in the activated ezrin binds to target membrane proteins either directly or indirectly through NHERF1 or 2, while the carboxy-terminal domain of about 32 amino acid residues of ezrin binds to cytoskeletal actin. The interaction of NHERF1 and ezrin is thus regulated by the autoinhibition and activation of ezrin.

Because ezrin and other ERM proteins bind to both cell membrane and the F-actin cytoskeleton, they contribute to membrane–cytoskeleton interface that influences a range of cellular functions, such as cell–cell adhesion, cell morphology, cell surface tension, and lateral mobility and exocytosis/endocytosis of the assembled transmembrane protein complexes. The manner that ezrin binds to the cytoskeletal actin could also control the spacing and movement of the membrane protein complexes that ezrin binds directly or indirectly via NHERF1 or NHERF2. The ERM proteins are responsible for generating specialized membrane domains and structures such as membrane ruffles and microvilli, which host a large variety of transmembrane channels, transporters, and receptors (Bretscher et al., 2002; Gautreau et al., 2002; Fehon et al., 2010). Ezrin is involved in

the formation of the immunological synapse and in T cell activation (Roumier et al., 2001). The interactions of the ezrin/radixin/moesin family proteins with the cell membranes and with the cytoskeletal actin facilitate the transmission of human immunodeficiency virus (HIV) into uninfected cells (Liu et al., 2009; Wong and Gough, 2009). There is also increasing evidence that ezrin promotes cancer metastasis and progression (McClatchey, 2003; Curto and McClatchey, 2004; Khanna et al., 2004; Yu et al., 2004; Elliott et al., 2005).

The interaction of NHERF1 and ezrin is essential for the cell surface assembly and the normal function of membrane proteins. NHERF1 and ezrin interact and cooperate in regulating ion transport in epithelial cells. Disruption of this link diminishes cell surface expression of ion transport proteins or receptors, which destroys their ability to transport ions across the cell membrane or to transduce signals. Expressing NHERF1 without the carboxy-terminal EB domain in cells leads to the internalization of Na^+/H^+ exchanger 3 (NHE3) and abolishes ion transport activities of NHE3 (Weinman et al., 2003). Truncation of the EBD results in loss of functional expression of the sodium–potassium-ATPase transporter at the cell membrane (Lederer et al., 2003). Similarly, expressing NHERF1 in cells impedes antagonist-induced endocytosis of PTH1R, but deleting the EBD of NHERF1 results in otherwise inactive ligands to internalize PTH1R (Sneddon et al., 2003). NHERF and ezrin are thus key elements to transmit the regulation of receptor signaling and ion transport functions by the actin cytoskeletal network.

NHERF and ezrin are necessary to anchor CFTR to the cytoskeleton for the proper function of CFTR (Short et al., 1998). An organized actin cytoskeleton is necessary to retain CFTR in the cell membrane so that CFTR can function properly (Prat et al., 1999). In turn, NHERF1 over-expression-dependent increase of cytoskeleton organization is necessary for rescuing the $\Delta\text{F}508$ mutant of CFTR (Favia et al., 2009). Taken together, these studies suggest the important roles of NHERF1 and ezrin in the bidirectional communication between CFTR and the F-actin cytoskeleton.

In summary, NHERF1 is a scaffolding protein that binds to transmembrane proteins and assembles membrane protein complexes. The important feature of NHERF1 is its binding to ezrin and to other (ERM) proteins, thus integrating cell surface membrane protein complexes into the cytoskeletal F-actin network. Such interactions stabilize the

NHERF1-assembled complexes of receptors and/or ion transport proteins at the cell membrane, and thus influence the cellular trafficking of the membrane proteins that NHERF1 interacts with. As a result, the cytoskeletal actin network controls the surface expression and the assembly of membrane proteins that have crucial impacts on the cellular or physiological functions. Moreover, the transmission of signals by NHERF1-ezrin complexes could be bidirectional between the cell membrane and the cytoskeletal F-actin network. The NHERF1-ezrin-assembled membrane complexes could influence the cellular distribution, the assembly, and the dynamics of the F-actin network. The NHERF1-ezrin complexes are thus important connectors that transduce signals between the cell membrane and the cytoskeleton.

A. *Allosteric Modulation of NHERF1 to Assemble Membrane Complexes*

The integration of the NHERF1-ezrin-assembled membrane complexes into the F-actin filament fit into the emerging picture that the F-actin cytoskeleton and actin-associated adapter proteins underlying the cell membrane regulate the function of membrane complexes. The cytoskeletal actin filament has long been recognized to provide a network of barriers that hampers the diffusion of membrane complexes inside cell membranes (Lee et al., 2007). However, F-actin can also exert active control on regulating the assembly of membrane protein complexes. During such processes, the F-actin-associated adapter proteins and scaffolding proteins function as signal transducers. The interactions among these adapter proteins are regulated by the dynamic conformational changes upon posttranslational modification or binding to signaling lipids and to other proteins. The interactions among these adapter proteins, such as NHERF1 and ezrin, provide a means to relay allosteric signals from the F-actin cytoskeleton to the membrane for the effective control of the membrane assembly. Moreover, it is becoming increasingly evident that NHERF1 and ezrin are signal transducers through which the F-actin cytoskeleton organizes the assembly of membrane receptor and ion transport protein complexes allosterically.

Recent biochemical and biophysical experiments have provided detailed molecular mechanisms that ezrin positively modulates the interactions of the PDZ domains of NHERF1 to assemble multiprotein complexes in a cooperative fashion. Biophysical methods have been applied to

determine the stoichiometry and affinity of NHERF1 binding to the C-terminal domain of CFTR (Li et al., 2005). Both static light scattering and analytical ultracentrifugation experiments show that NHERF1 exists as monomer in solution. The PDZ1 domain of NHERF1 was found to have high binding affinity, while PDZ2 plus the C-terminal domain have a lower binding affinity for C-CFTR. However, when the FERM domain of ezrin binds to the carboxy-terminal EBD of NHERF1 with high affinity (with $K_d = 19$ nM), the binding affinity of PDZ2 for the last 70 amino acid residue CT domain of CFTR (C-CFTR), which contains a type I C-terminal PDZ-binding motif—DTRL, increases by 26-fold (see Fig. 2). As a result of EB, the stoichiometry of the full-length NHERF1 binding to C-CFTR is increased from 1:1 to 1:2. Moreover, the binding affinity of PDZ1 for the target protein also increases significantly upon FERM binding. A thermodynamic cycle analysis indicates that ezrin positively modulates the intramolecular domain–domain interactions in NHERF1 and controls NHERF1 to assemble membrane signaling complexes allosterically (Li et al., 2009) (see Fig. 3).

EB to NHERF1 also positively regulates the interactions of NHERF1 with other signaling proteins, such as PDZK1, which is a four PDZ domain scaffolding protein that belongs to the NHERF family of proteins (LaLonde et al., 2010). The binding of the PDZ domains of NHERF1 to PDZK1 in turn disrupts the autoinhibition-like interactions in PDZK1 to enable it to assemble larger protein complexes that contribute to cellular microvillar organization (LaLonde and Bretscher, 2009). In addition, EB can also activate NHERF1 to assemble a heterogeneous complex, PTEN at PDZ1 and β -catenin at PDZ2 (Morales et al., 2007).

B. Negative Cooperativity and Feedback Loop

NHERF1 can also send negative feedback to the network through domain–domain interactions. In the presence of C-CFTR in the PDZ1 domain of NHERF reduces the affinity of the NHERF C-terminus for FERM by sixfold (Li et al., 2005). The reduction in binding affinity of NHERF1 for ezrin suggests that binding of C-CFTR to the PDZ1 domain of NHERF can negatively regulate the interaction of NHERF with ezrin. The weakened NHERF–ezrin interaction, due to the binding of CFTR to the PDZ1 domain of NHERF, can also serve as a feedback loop to weaken the interaction of the PDZ2 domain with CFTR, by uncoupling EB

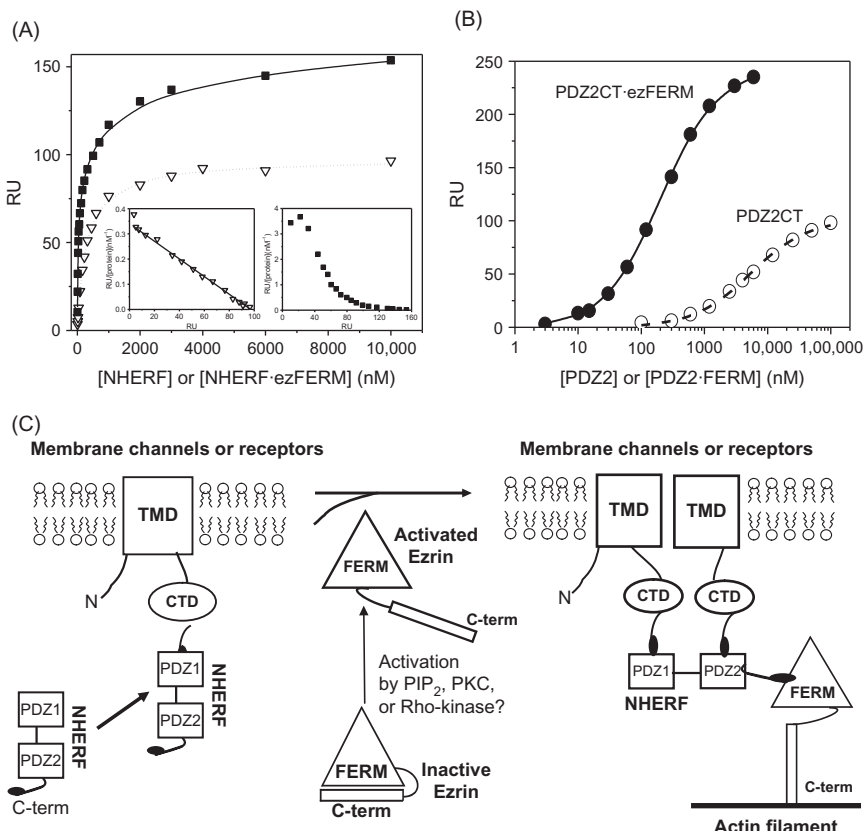


FIG. 2. (A) SPR analysis indicates increased affinity and stoichiometry of C-CFTR binding to NHERF1 when the FERM of ezrin is bound to NHERF1. (∇) NHERF1 alone binding to C-CFTR is monovalent as shown by the linear Scatchard plot (inset). (\blacksquare) NHERF-FERM binding to C-CFTR is bivalent as also shown by the nonlinear Scatchard plot (inset). (B) Increased binding affinity of C-CFTR for PDZ2, when FERM is bound to the PDZ2CT construct. Note that in (B), the bindings of both PDZ2CT and PDZ2CT-FERM to C-CFTR have reached saturation. The X-axis is in logarithmic scale in order to show both binding curves in the same plot. (C) Our hypothesis about the regulation of NHERF1 by ezrin, which changes the stoichiometry of NHERF interaction with membrane channels or receptors. *TMD*, transmembrane domain; *CTD*, the cytoplasmic domain. Ezrin binding to the C-terminus of NHERF activates PDZ2 to interact tightly with the cytoplasmic domain of channels or receptors. The schematic also shows that the C-terminus of ezrin binds to the filamentous actin.

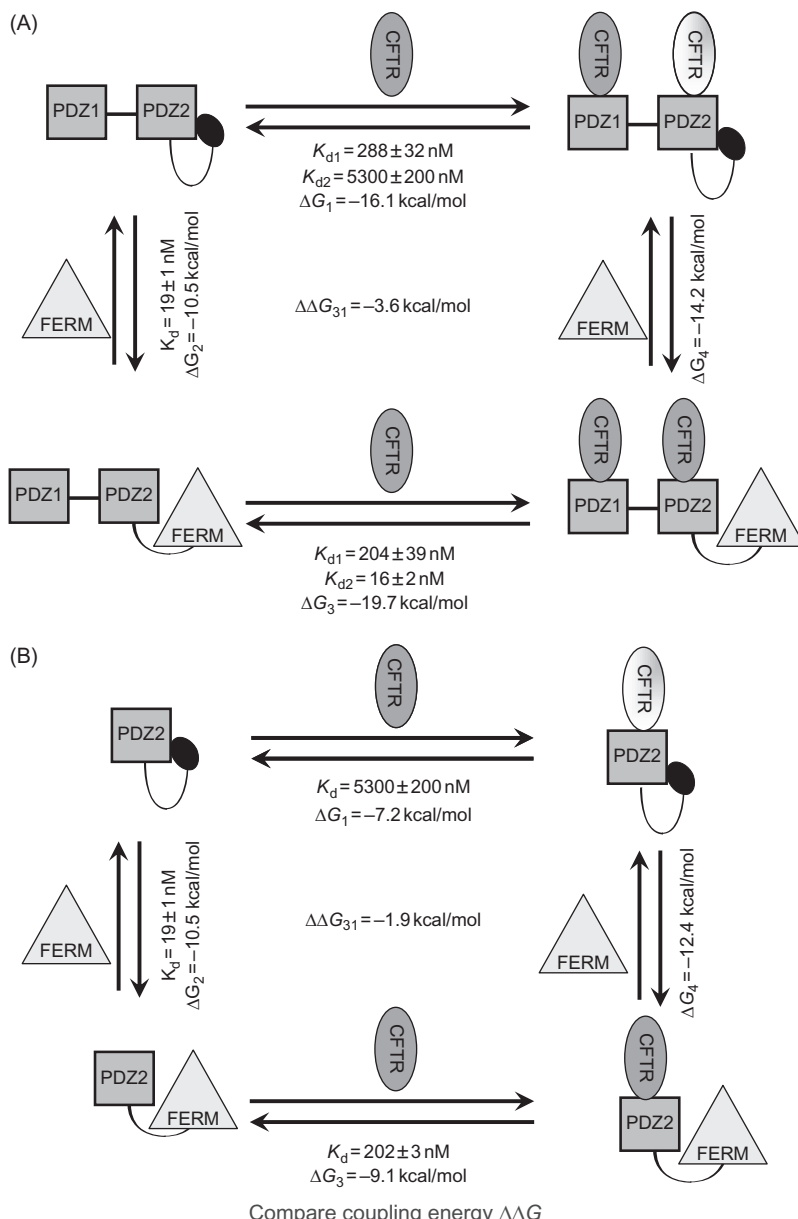


FIG. 3. Thermodynamic cycle analysis reveals FERM-induced long-range interdomain allostery in the scaffolding protein NHERF1. FERM binding to NHERF1 increases the binding affinities of both PDZ1 and PDZ2 for C-CFTR. (A) The “coupling”

to NHERF. As a result, the stimulation of CFTR channel due to the activation of NHERF by ezrin is weakened.

NHERF1 also displays both positive and negative long-range allosteric communications between its two PDZ domains. A study by LaLonde et al. (2010) shows that mutations in PDZ1 reduce the binding affinity of PDZ2, or occupancy of a ligand in PDZ1 enhances the binding capability of PDZ2. Intriguingly, a recent study by Garbett et al. (2010) shows that serine to aspartic acid mutations in NHERF1, which mimic phosphorylation at S280 and 302 by cdc42 or phosphorylation at S162,339 and 340 by PKC inhibits ligand accessibility to PDZ1 when PDZ2 is occupied, suggesting that NHERF1 phosphorylation by either PKC or Cdc2 inhibits simultaneous binding to both PDZ domains.

These studies indicate that there are long-range domain–domain allosteric communications in NHERF1. Adapter and scaffolding proteins, NHERF1 and ezrin are thus not just passive adapters to dock the binding partners. Instead, ezrin and NHERF function as signal transducers between cell membranes and the actin cytoskeleton. The cortical actin cytoskeleton is thus not only a passive support of cell membranes but also actively controls the assembly of membrane proteins. F-actin and associated membrane–cytoskeleton adapter or scaffolding proteins thus integrate diverse signals in space and time to influence all aspects of biology from receptor signaling to cellular homeostasis (Pollard and Cooper, 2009).

The allosteric regulation of membrane protein–NHERF1–ezrin–actin cytoskeleton is bidirectional. The above cases show inside-out types of regulation that transmits the control signal of membrane assembly by the cytoskeletal F-actin. The NHERF1·ezrin can also transmit outside-in type signals. The NHEF1·ezrin complex allosterically assembles the CFTR homo and/or hetero complexes and anchors the assembled complexes to the F-action cytoskeleton, which promote the surface expression and cross

energy (Fersht, 1998) for FERM binding to the NHERF1 carboxy-terminus and for NHERF binding to C-CFTR is $\Delta\Delta G = \Delta G_3 - \Delta G_1 = \Delta G_4 - \Delta G_2 = -3.64$ kcal/mol. K_d values, taken from our previous publication, are measured by surface plasmon resonance (Li et al., 2005). (B) The coupling energy for FERM binding to PDZ2CT and for PDZ2CT binding to C-CFTR is $\Delta\Delta G = -1.93$ kcal/mol. Comparing the coupling energy of C-CFTR binding to the full-length NHERF1 with that of binding to PDZ2CT suggests that FERM binding induces long-range allosteric-binding behavior in NHERF.

talk signaling of CFTR. Alternatively, anchoring ion transport proteins to the cytoskeleton alters the organization and assembly of cytoskeletal actin, and is believed to influence cell shapes and the ability of a cell to migrate (Denker and Barber, 2002). Similarly, disruption of the interactions of podocalyxin/NHERF2/actin cytoskeleton results in loss of glomerular foot processes and the glomerular disease proteinuria in animal models (Takeda et al., 2001). For instance, podocalyxin activates *RhoA* and induces actin reorganization through NHERF1 and ezrin (Schmieder et al., 2004). The NHERF1-ezrin complex promotes β PDGFR signaling that results in actin cytoskeletal rearrangements to the cytoskeleton and promote cell spreading and migration (James et al., 2004).

IV. STRUCTURAL BASIS OF AUTOINHIBITION AND LONG-RANGE ALLOSTERY IN NHERF1

The above examples show that the assembly of membrane complexes by NHERF1 is allosterically regulated. The allosteric regulation is not confined to a single protein, but rather it is an allosteric relay of signals through a chain of multiple protein-protein interactions. Such a relay of signals, in a Rube Goldberg device style, can also be found in almost all other signaling pathways (Ma and Nussinov, 2009; Scott and Pawson, 2009). The relay of signals, using multiple proteins as transistors, has the advantage of being much more efficient and specific than thermal diffusion in transmitting regulatory signals from one location to a reach a target. Because of the multiple domains of NHERF1, EB activation of PDZ domains enable NHERF1 to assemble homo and/or hetero membrane complexes, thus integrating signals to promote cross talks among membrane proteins. In return, binding to NHERF1 could enhance the binding of ezrin to the F-actin filament, thus integrating the membrane signals to the cytoskeleton network. The regulated complex formation between NHERF1 and ezrin in the membrane-cytoskeleton thus provide an excellent prototype to understand how multiple proteins interact to form complexes, transmit and relay signals.

We next review structural and dynamic studies of NHERF1 and its interactions with ezrin with an emphasis on understanding the long-range allosteric binding communicated through interdomain conformational changes (Li et al., 2009; Bhattacharya et al., 2010). Our recent study using NSE spectroscopy reveals that interdomain motions among PDZ1,

PDZ2, and CT in NHERF1 on nanometer length scales and on submicrosecond timescale can propagate allosteric-binding signals dynamically (Farago et al., 2010). The long-range conformational changes and nanoscale dynamics during the interactions of NHERF1 and ezrin provide a first glimpse for understanding the mechanisms of how cellular signals are transmitted allosterically over a long distance in the signaling network.

A. *NHERF1 Has a Highly Elongated Shape, Allowing Long-Range Interdomain Allosteric Communications*

Understanding the scaffolding function of a multidomain protein requires the structure of the full-length protein. Because of the quite large size and the dynamic nature, the structure of the full-length NHERF1 has eluded high-resolution structural studies. Combining solution small angle X-ray scattering (SAXS) with high-resolution structure data on the fragment can provide information about the 3D shape, domain–domain distances, and domain orientation of such heterogeneous multidomain proteins (Bu et al., 1998; Bu and Engelman, 1999). The structural information from SAXS on the full-length scaffolding protein NHERF1, although at low resolution, is accurate and necessary to understand how NHERF1 and other scaffolding proteins assemble complexes.

NHERF1 is monomeric in solution at concentrations as high as 2 mg/ml (corresponding to 50 μ M) as determined by a combination of gel filtration, static and dynamic light scattering, and analytical ultracentrifugation experiments (Li et al., 2005, 2007a, 2009; Garbett et al., 2010). Above 3 mg/ml, NHERF1 starts to show a small fraction of weak association in light-scattering experiments, but analytical ultracentrifugation suggests that NHERF1 is a monomer even at higher concentrations (Li and Bu, unpublished data). A recent study shows that NHERF1 is an elongated monomer regardless of the phosphorylation states (Gabbett et al., 2010).

SAXS provides the 3D shape of NHERF1 and the spatial arrangement of the different domains in NHERF1 (Li et al., 2005, 2007a, 2009). The 3D molecular shape of NHERF1 shows that the full-length NHERF1 monomer is elongated. The elongated shape of NHERF1 is also manifested by the very asymmetric shape of the length distribution function $P(r)$ obtained from SAXS experiments with a maximum dimension of 140 Å (Fig. 4). The radius of gyration (R_g) of NHERF1 is 40.9 ± 0.6 Å.

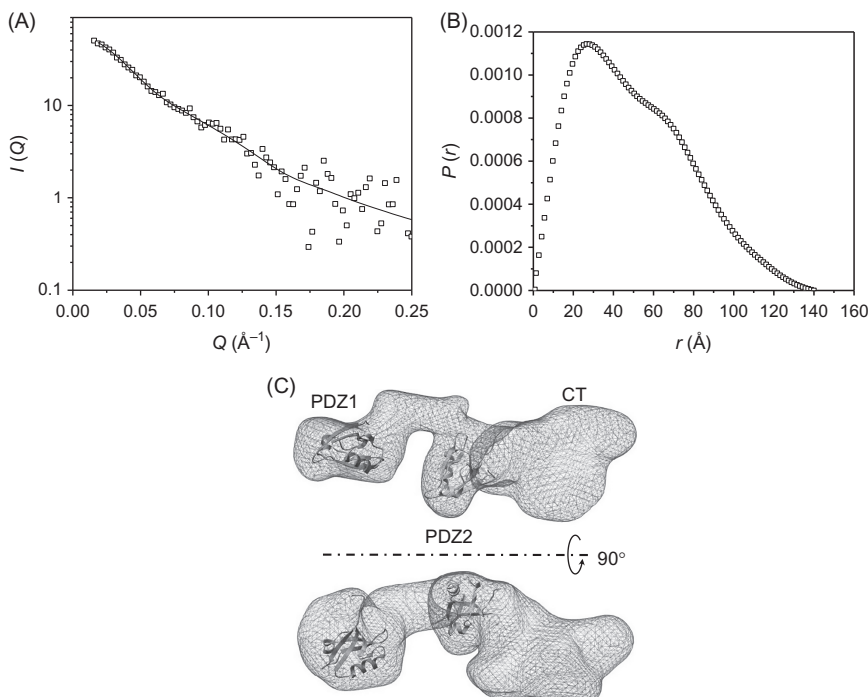


FIG. 4. Solution small angle X-ray reveals the 3D shape of full-length NHERF1. (A) SAXS data of the scattered intensity $I(Q)$ versus Q . (B) Length distribution function $P(r)$. (C) 3D shape of NHERF1 reconstructed from SAXS data using the program DAMMIN (Svergun, 1999).

There are three lobes in the 3D map of NHERF1 reconstructed from SAXS. The lobe representing the PDZ1 domain is well separated from the other two lobes. The two lobes representing PDZ2 and CT domains are in close contact with each other, indicating that there are domain–domain interactions between PDZ2 and CT (Li et al., 2005, 2007a). The center-of-mass distance between PDZ2 and CT is 45.8 Å. The distance between PDZ1 and PDZ2 is 57.1 Å, and the distance between PDZ1 and CT is about 110 Å.

In the 3D map of NHERF1, the lobe representing the CT domain is compact with a clearly defined boundary. Our NMR studies find that the CT domain is largely unstructured (Bhattacharya et al., 2010). Combining the SAXS and NMR results suggests that the CT domain adopts a compact but disordered conformation in NHERF1.

Because of the elongated shape of NHERF1, the PDZ1 domain is separated about 110 Å away from the CT domain (Li et al., 2007a, 2009). PDZ1 and CT are unlikely to form head-to-tail like interactions as previously thought. Rather, the modulation of the binding capability of PDZ1 by FERM binding at a remote site is through a long-range allosteric behavior.

B. Allosteric Control in NHERF1 Originates from Domain–Domain Interactions

Small angle neutron scattering (SANS) has the unique advantage of allowing the structure of multicomponent complexes by contrast variation and deuterium labeling. The technique of contrast variation neutron scattering relies on the tremendous scattering difference between hydrogen and deuterium. By selectively labeling portions of a protein or a complex with deuterium, and changing the D₂O composition of buffer, the subunit can be made essentially invisible to neutrons at the contrast match point. Thus, one can highlight the component of interest for study. This feature of neutron scattering makes it particularly useful for studying the structure of biological macromolecular complexes. SANS thus has the advantage of studying the structure of multicomponent complexes by contrast variation and deuterium labeling. This critical feature of neutron scattering makes it particularly useful for studying biological macromolecular complexes.

We have used SANS to determine the conformational changes of NHERF1 upon forming a complex with ezrin, using deuterated NHERF1 and hydrogenated FERM domain (Li et al., 2009). Contrast variation SANS reveals that when FERM binds to the C-terminus of NHERF1, FERM induces large conformational changes in NHERF1. The shape of the length distribution function $P(r)$ of NHERF1 in the complex is significantly different from that in solution (Fig. 5). The radius of gyration changes 40.9 ± 0.6 Å in solution to 45.8 ± 0.8 Å in the complex, but the change in D_{\max} is less dramatic from 140 to 145 Å. This result suggests a significant change in the geometry and size of NHERF1.

Comparing the 3D shape of ^dNHERF1 in solution and in the complex shows that the region linking PDZ2 and CT becomes more extended in NHERF1 (Fig. 5). An angle of about 120° is formed between PDZ1–PDZ2 and PDZ2–CT at the location of PDZ2 in ^dNHERF1 in the complex, which

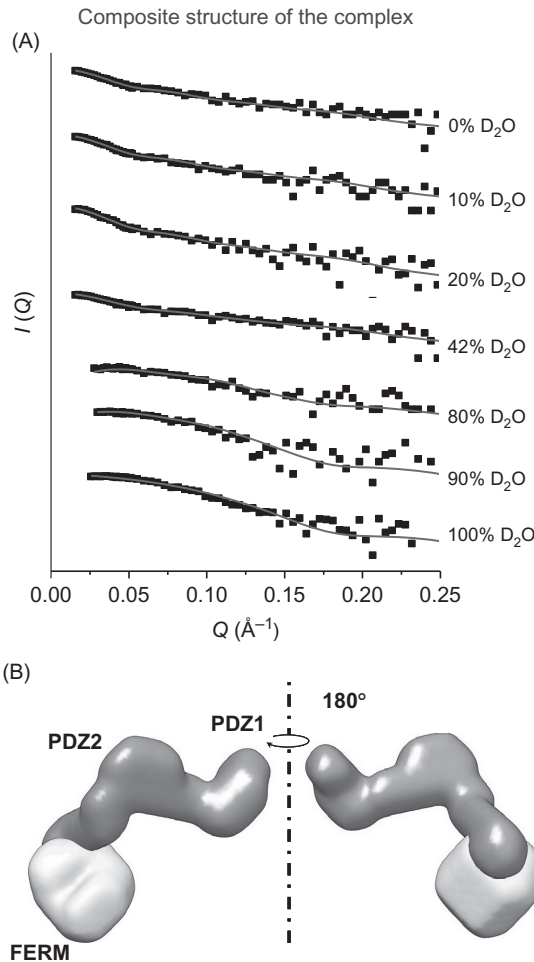


FIG. 5. Contrast variation SANS reveals the composite structure of the deuterated NHERF in complex with unlabeled FERM ($^d\text{NHERF1}\cdot\text{FERM}$) complex. (A) SANS data of $^d\text{NHERF1}\cdot\text{FERM}$ at various contrasts. The lines are fits to the scattering curves when reconstructing the 3D composite structure of the complex. The χ^2 values of fitting are shown in the plots. (B) The 3D models of the $^d\text{NHERF1}\cdot\text{FERM}$ reconstructed *ab initio* from contrast variation SANS (Petoukhov and Svergun, 2006).

is consistent with the $P(r)$ shape changes of d NHERF1 in the FERM-bound complex. The distance between the centers of PDZ2 and the EBD changes from 45.8 Å in solution to 63 Å in the complex, suggesting that domain-domain contacts between PDZ2 and CT are disrupted.

Significant conformational changes are also apparent in the region that links PDZ1 and PDZ2. The distance between PDZ1 and PDZ2 changes from 57.1 Å in solution to 67.0 Å in the complex. In addition, the SANS results also suggest that the FERM domain does not have global conformational changes when it is bound to NHERF1. The SANS results thus provide a structural explanation of the binding and thermodynamic analyses, which demonstrate positive allosteric regulation of NHERF1 by ezrin as it assembles membrane protein complexes.

C. Redefinition of the Structural Boundary of PDZ Domains

The structures of the isolated PDZ1, PDZ2 of domains of NHERF1, and the structures of the NHERF1 PDZ1 domain in complex with the carboxy-terminal peptides of membrane receptors and channels have been determined by X-ray crystallography (Karthikeyan et al., 2001, 2002). The putative NHERF1 PDZ structures adopt similar fold as in other PDZ proteins. The PDZ domains have a characteristic β-sandwich structure that is composed of six strands stacked in an antiparallel fashion into two β-sheets, which are flanked by two α1 and α2 helices (Fig. 6). The partially open hydrophobic cavity enclosed by the β-sandwich (Fig. 6) serves as a robust scaffold to recruit peptide based ligands. The conformation of the carboxylate binding (CB) loop (–GYGF–) is capable of forming H-bond pairs with the peptide ligand (Doyle et al., 1996). Primary sequence analysis predicts the “conventional” PDZ1 domain of NHERF1 starts amino acid L14 and ends at D92, and the PDZ2 domain starts at L154 and ends at V231.

However, our NMR structural studies on a larger PDZ2 plus the CT domain (PDZ2CT) find that, besides the putative PDZ2 structure, the structured region of NHERF1 PDZ2 extends to N252, well beyond V231 at the predicted boundary for a putative PDZ domain (Fig. 6) (Bhattacharya et al., 2010). We find that a C-terminal extension (R233–N252) consists of two helices α3 and α4, forming a closed hydrophobic cluster at the C-terminal end of the putative PDZ fold. Thus, the C-terminal extension is an integral part of the PDZ2 domain. The extended

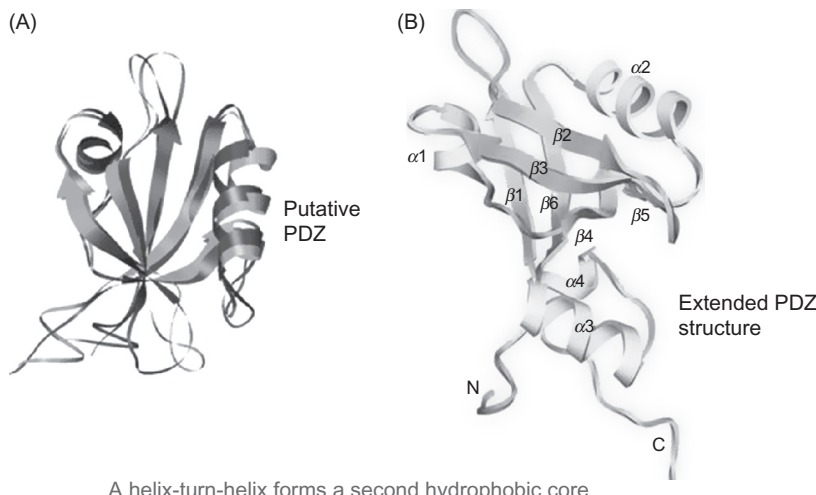


FIG. 6. The extended structure of PDZ2 of NHERF1 with a novel helix-turn-helix subdomain at the carboxy-terminal end of the putative PDZ fold. (A) The structure of a putative PDZ domain (PDB code: 2JXO). (B) The extended structure of PDZ2+²⁷⁰ with a C-terminal helix-turn-helix motif (PDB code: 2KJD).

PDZ structure is thermodynamically more stable, and has higher affinity for ligand than the putative PDZ²⁴⁰. Because the helical extension does not interact with the ligand, this extension augments the PDZ2 stability and affinity for ligands by an allosteric mechanism instead of direct engagement.

The C-terminal helical extension of a PDZ fold appears to be a feature that is frequently shared by many PDZ domains (Bhattacharya et al., 2010). Based on multiple sequence alignment alone, the carboxy-terminal hydrophobic residues are conserved across all the PDZ domains in the NHERF family of proteins, suggesting similar functional roles for this extended helical fold (Bhattacharya et al., 2010). Moreover, multiple alignment and secondary structure analysis predict α -helical propensity at the C-terminal end in a majority of the PDZ domains that we have analyzed even though the amino acid sequence at the C-terminal extension is not well conserved. The C-terminal helical extensions have been found in many of the PDZ domains that are important in cell signaling, such as those of the human harmonin, protein tyrosine phosphatase, tamalin and PARR3, and PDZ1

of PSD-95, as well as the PDZ domains of *Drosophila melanogaster* INAD (Bhattacharya et al., 2010). In addition to regulating the target affinity, the C-terminal extensions to PDZ domains are also known to mediate multimerization in some examples such as harmonin (Verpy et al., 2000; Wang et al., 2010). Thus, amino acid sequence variation within a PDZ domain or in the PDZ-binding motif is not the only means to render specificity for PDZ/target protein interactions. The structure flanking the core PDZ fold can also influence target peptide binding. The roles of the extended structure(s) may include modification of “dynamic allostery.”

D. Autoinhibition of PDZ2 by the C-Terminal Domain of NHERF1

The NMR structure of the PDZ2CT structure reveals that a PDZ-binding motif (-SNL) located at the C-terminus of NHERF1 binds to the ligand-interaction pocket of PDZ2 (Bhattacharya et al., 2010). The NMR structure thus corroborates the biochemical data that there are autoinhibitory interactions between PDZ2 and the CT domain of NHERF1 (Morales et al., 2007; Li et al., 2009). While NMR and circular dichroism indicate that the CT domain of more than 100 amino acid residues adopts a largely disordered structure, SAXS shows that this CT domain is a collapsed domain. When binding to the FERM domain of ezrin, the EBD, which resides in the CT domain and overlaps with the C-terminal PDZ-binding motif, adopts a distinct helical structure (Terawaki et al., 2006), but the linker region between PDZ2 and EBD becomes totally unfolded (Bhattacharya et al., 2010). The binding affinity between FERM and EBD is strong with $K_d = 10 \text{ nM}$. Binding to FERM domain thus disrupts the autoinhibition between PDZ2 and CT domain, and the disordered linker region acts as a flexible spacer between PDZ2 and the FERM domain.

E. Disease-Associated NHERF1 Mutations Affect the Structure, Stability, and Binding Capability of PDZ Domains

Using NMR and biophysical experiments, we have analyzed the effects of the disease-associated R153Q and E225K mutations on protein structure and stability (Bhattacharya et al., 2010). These mutations were identified in patients with impaired renal phosphate reabsorption (Karim et al., 2008). The R153Q and E225K mutations are located in

PDZ2 outside the ligand-binding sites (Bhattacharya et al., 2010). The R153Q mutant is considerably less stable (with an unfolding transition temperature $T_m = 37^\circ\text{C}$) than the wild-type protein ($T_m = 55^\circ\text{C}$) (Bhattacharya et al., 2010), due to the loss of H-bond/salt bridge between the positively charged bidentate R153 N^{l} group in strand $\beta 1$ and the negative charge of the COO^- groups of D197 ($\beta 4$) and D232 at the N-terminus of $\alpha 2$ helix. The binding affinity of R153Q for the peptide ligand has also decreased.

The E225K mutation has a dramatic effect on the conformational stability of PDZ2 domain and this mutant fails to express as an intact protein in *Escherichia coli* at either 37 or 20 °C. In the wild-type protein, the negatively charged E225 is complemented by surrounding positive charge of lysine side-chains (K158 and K227) on the exposed surface of the β -sheet (Bhattacharya et al., 2010). The unfavorable electrostatic energy of the E225K mutant would destabilize the protein.

Thus, although these mutations are located outside the ligand-binding site of the PDZ2 domain, the mutations R153Q and E225K evidently destabilize the native state and would therefore accelerate degradation in a cellular context. Reduced protein stability could translate into the loss of functional NHERF1 expressed in cells, and diminish the ability of NHERF1 to assemble transmembrane protein complexes of NPT2a at the cell membrane.

V. DYNAMIC PROPAGATION OF ALLOSTERIC SIGNALS BY NANOSCALE PROTEIN MOTION

The above examples demonstrate that allosteric signals are transmitted over a long distance within a single protein, as well as in multiple protein–protein interactions. There is increasing evidence that the transmission of allosteric-binding signals requires both conformational changes and protein motion (Kern and Zuiderweg, 2003). Protein dynamics can initiate and control protein function. Protein motion regulates the transition state dynamics of enzyme catalysis (Benkovic and Hammes-Schiffer, 2003; Eisenmesser et al., 2005), and protein motion has been proposed to contribute significantly to the propagation of allosteric signals (Cooper and Dryden, 1984). Information arising from ligand binding can be communicated to a distal site in a protein by altering internal dynamic modes (Hawkins and McLeish, 2004).

Most studies have been focused on how allosteric signals are transmitted within a single protein domain, such as in the PDZ domains. However, the overall dynamic architectures, and in particular the long-range motion properties of scaffolding proteins that control the function of assembled macromolecular signaling complexes, remain a largely unexplored territory. Protein motions on nanoscales are indispensable for relaying signals allosterically in the cellular networks (Ma and Nussinov, 2009). This concept is emerging as a powerful theme in cell signaling. To understand the mechanism of how allosteric signals are propagated in multidomain proteins and over a cascade of multiple protein–protein interactions requires the study of structure and dynamics on nanolength scales that are comparable to the dimension of multidomain signaling proteins such as in NHERF1 and ezrin.

In the following, we first summarize our new applications of NSE spectroscopy to studying nanoscale long-range domain motions in NHERF1 upon forming a complex with ezrin. We expect that NSE can be extended to determine how signals are propagated in multiprotein signaling complexes.

A. *The Physical Concepts Behind Protein Dynamics*

Many experimental studies show that it is sensible to attribute the dynamic properties of bulk materials to proteins (Howard, 2001). For example, the Young's moduli of proteins are typically found to be mechanically isotropic, independent of the direction of the applied force (Howard, 2001, chapter 8). Moreover, mechanical measurements show that the Young's moduli of very different proteins are fairly similar (Howard, 2001, Table 3.2, page 31), supporting the notion that proteins can often be thought of as being largely composed of fairly uniform soft matter. According to the domain concept of structural biology (Creighton, 1993), multidomain proteins can be considered as being comprised of somewhat rigid domains connected by soft spring linkers (Gerstein et al., 1994; Zaccai, 2000; Farago et al., 2010). The conceptual virtue of attributing materials properties to proteins can easily be seen by comparing the difficulty of retaining an atomic-level description, whereby one must perform difficult molecular dynamics simulations to achieve an understanding of protein motion that may provide only a limited improvement over the materials point of view.

1. Protein Motions Are Overdamped, Creeping Movements Rather than Underdamped Oscillations

The environment in which proteins act is one of low Reynolds number (usually abbreviated Re). The Reynolds number (which was actually introduced by Stokes!) is the ratio of the magnitude of inertial forces to that of the forces that arise from the viscous drag that opposes motion. If inertial forces are more important, Reynolds number is large, and forces are proportional to mass times acceleration. If viscous drag is more important, the Reynolds number is small, and mechanical forces are proportional to the velocity of the protein (more generally incorporating a concept known as the mobility tensor, which we will discuss in detail below). Reynolds number is actually an imprecise concept, usually used as a way to argue that certain terms in the Navier–Stokes equations of fluid dynamics can safely be neglected. Reynolds number can be *estimated* by the simple formula $Re=Lv/\nu$, where L is a characteristic length scale of the protein, v is a characteristic velocity, and ν is the kinetic viscosity of the solvent (for water, $\nu=10^5 \text{ \AA}^2/\text{ns}$). At large Re , one has oscillatory (underdamped) phenomena such as the ringing of a bell, while at small Re (which occurs when Re is less than about 1000), dynamics involves slow, creeping *overdamped* motion.

The Reynolds number for typical proteins is less than 0.1, indicating that they are well within the low Re regime. Simple calculations show that even a multiprotein complex as large as a ribosome is still in the overdamped regime (Howard, 2001, page 43). The environment of a protein thus has more in common with playing badminton at the bottom of a swimming pool full of molasses (low Re) than in crossing the Atlantic in an ocean liner (high Re), see reference Howard (2001, chapter 3 and Table 3.4). Since for proteins, inertial forces are less important than diffusive, viscous effects, protein dynamics should be largely independent of the mass of the protein (or of the relative masses of internal domains). For example, the diffusion constant of a deuterated protein should be almost the same as a hydrogenated protein, even though deuterium has twice the mass of hydrogen. This effect will be seen to be important for our later discussion of deuterium contrast matching.

Proteins obey Brownian dynamics. Protein dynamics arises as a result of interplay between the mechanical forces mentioned above, and the thermal forces that arise from the collision of the protein with solvent

molecules. These thermal forces are random in magnitude and direction, and lead to the protein undergoing a process known as *diffusion*. A freely diffusing object displays what is called *Brownian motion*, with frequent changes in the direction and speed of its movement. The world in which proteins operate is therefore characterized by the presence of a significant amount of noise and the resultant diffusion of protein subunits arising from thermal motion. This thermal motion is essential for the protein to reach its equilibrium state.

The limiting rate for the propagation of conformational changes is the speed of sound in proteins. This is true even in the case of overdamped motion, see reference Howard (2001, page 307). We can estimate the speed of sound by $c \approx \sqrt{E/\rho}$, where $E \approx 1$ GPa is the Young's modulus of a protein, and $\rho \approx 10^3$ kg/m³ is the density of protein. A crude estimate of the limiting speed of conformational change is thus 10^4 Å/ns. Since most proteins are of the order of a few hundred Angstroms in size, we see that long-range coupled motion between separate protein domains is physically possible on nanosecond timescales.

Protein dynamics involves a hierarchy of length scales and timescales. Biologically relevant protein motions occur on timescales ranging from femtoseconds to hundreds of seconds and from sub-Angstrom length scales up to hundreds of Angstroms. Small-amplitude local conformational changes (partially directed by mechanical forces) drive a protein to explore its energy landscape and find the saddle-like passes between energy valleys. These semideterministic *local* motions inspire larger scale stochastic *global* conformational changes between these valleys. The small-scale local dynamic motions are typically on the picosecond-to-nanosecond timescale, while the global kinetic motions are generally of the order of microseconds to milliseconds or longer (Lindorff-Larsen et al., 2005; Fehon, 2006). The existence and nature of the motions in this hierarchy are summarized in Table I.

B. Nanoscale Protein Dynamics: The Emergence of a New Frontier

Although the importance of protein domain dynamics has long been recognized, it has only been in recent years that the field has burgeoned. This situation arises in part from two causes. First, there has been a shortage of methods that are capable of addressing such a complicated issue. Second, the theoretical methods needed to understand protein

TABLE I
The Hierarchy of Protein Dynamics (Gerstein et al., 1994; Palmer, 2004)

Types of motion	Function	Timescale	Amplitude
<i>Local motions</i>	Ligand docking flexibility	Femtoseconds (fs) to picoseconds (ps)	$< 1 \text{ \AA}$
Atomic fluctuation	Thermal diffusion	$10^{-15}\text{--}10^{-12} \text{ s}$	
Side-chain motion	Active site conformation adaptation	Nanoseconds (ns) to microseconds (μs)	$1\text{--}5 \text{ \AA}$
<i>Medium-scale motions</i>		$10^{-9}\text{--}10^{-6} \text{ s}$	
Loop motion	Binding Specificity	Microseconds (μs) to milliseconds (ms)	$5\text{--}10 \text{ \AA}$
Rigid-body motion	Hinge-bending motion		
<i>Large-scale motions</i>	Allosteric transitions		
Domain motion			
Subunit motion	Ligand-binding, protein-protein interaction	Milliseconds (ms) to hours	$> 10 \text{ \AA}$
<i>Folding-unfolding transition</i>		$10^{-3}\text{--}10^4 \text{ s}$	

dynamics (which have their origins in the study of polymers) have only been developed recently.

Biophysical techniques: the promise of neutron scattering. The observation of protein motion on nanometer length scales and on nanosecond to microsecond timescales has remained an elusive goal because this is a spatial-temporal regime that has not been reached by existing biophysical techniques. Thus there is an important information gap, on nanoscales, between the structural dynamics occurring at atomic resolution and the cellular organization and dynamics on the much larger micron length scales and slower timescales. This information gap is both spatial and temporal. One technique of great promise for addressing this knowledge gap is neutron scattering (Higgins and Benoit, 1994), which is emerging as a powerful way to address protein dynamics. The neutron appears as a natural candidate for the study of proteins, as thermal neutrons possess a wavelength that is of the order of Angstroms, making it an appropriate probe for protein structure. Moreover, the existence of such tools as contrast matching is unique to this field. We illustrate this concept with an example shown in Fig. 7.

In a multicomponent contrast-matching experiment, one can selectively deuterate a particular protein domain or a subunit in a complex (Fig. 7). In D_2O buffer solution in which the NSE experiments are conducted, the deuterated component becomes invisible to neutron. Since deuteration should not significantly affect protein dynamics, despite the fact that deuterium has about twice the mass of hydrogen.

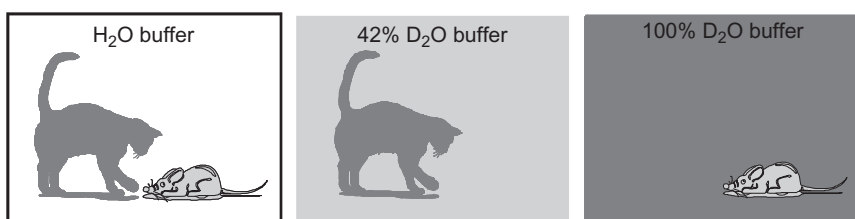


FIG. 7. Contrast variation in neutron-scattering experiments from a protein complex with selective deuteration of one subunit. (A) In H_2O buffer solution, both the deuterated cat and hydrogenated mouse scatter neutrons. (B) In 42% D_2O at the contrast match point of hydrogenated component (hydrogenated mouse), only the deuterated component (cat) scatters neutron. (C) In 100% D_2O buffer and at the match point deuterated component (cat), only the hydrogenated component (mouse) scatter neutron. The deuterated component (cat) is invisible to neutrons.

So why were neutrons not used more extensively? The answer is largely historical (Higgins and Benoit, 1994). The neutron was first discovered by Chadwick in 1932, and the first nuclear reactors were built during the 1940s and 1950s. However, the first scientists to use these reactors for research were solid state physicists employed at the reactor centers themselves. The high-flux reactors needed for polymer science were designed and built in the USA and France during the late 1960s, and slowly became available (and of interest) to polymer scientists. Today, there are a number of research reactors and neutron scattering centers worldwide. There are a number of spectrometric techniques, such as time-of-flight and backscattering, in addition to NSE spectroscopy. NSE is possibly the most powerful technique available today for the study of protein dynamics. (It is also the rarest, as there are only a handful of NSE spectrometers in the world!).

The development of theoretical techniques for protein dynamics. Concomitant with the rise of experimental techniques for the study of polymer dynamics, the theoretical technology need to understand the experimental results began to emerge. As will be explicated below, the theory behind protein dynamics emerges as a natural (if significantly more complex) extension of the theoretical framework developed for understanding polymer dynamics. Readers interested in a detailed look at this fascinating field may find (Berne and Pecora, 1976; Doi and Edwards, 1986) useful for further study. We present here only a summary of the basic ideas. We begin by considering the interpretation of experimental results from NSE spectroscopy. Although it is perhaps the most difficult experimental technique to understand, the results lend themselves to easy interpretation.

NSE measures the intermediate scattering function $I(Q,t)$, which is the spatial Fourier transformation of the space-time van Hove correlation function $G(r,t)$ (Mezei, 1980), $I(Q,t) = \int_V G(r,t) \exp(-iQ \cdot r) dr$, where $Q = (4\pi \sin(\theta/2))/\lambda$ is the magnitude of the scattering vector with θ the scattering angle, λ the wavelength of the neutron, t is the time, and r is the position of a scattering center. (The designation “intermediate” arises precisely because only one of the variables of $G(r,t)$ is Fourier transformed.) Like the static SAXS, in the low Q region, $I(Q,t)$ is dominated by coherent scattering that yields the cross-correlation $G(r,t)$, that is, the probability of finding a nucleus at position r_i at time $t=0$ and finding another nucleus at position r_j at time t .

For a given Q , $I(Q,t)$ typically can be fit to a single exponential in time (and is difficult to fit to more exponentials). A natural way to interpret

neutron-scattering data is therefore to examine the effective diffusion constant $D_{\text{eff}}(Q)$ as a function of Q , which is determined by the normalized intermediate scattering function $I(Q,t)/I(Q,0)$:

$$\begin{aligned}\Gamma(Q) &= -\lim_{t \rightarrow 0} \frac{\partial}{\partial t} \ln[I(Q, t)/I(Q, 0)] \\ D_{\text{eff}}(Q) &= \frac{\Gamma(Q)}{Q^2}\end{aligned}\quad (1)$$

where $I(Q,0)$ is the static form factor. As $I(Q,t)/I(Q,0)$ is generally amenable to a single-exponential fit in time (see Fig. 1), $D_{\text{eff}}(Q)$ can be accurately estimated by the first cumulant expression (Bu et al., 2005):

$$D_{\text{eff}}(Q) = \frac{k_B T}{Q^2} \frac{\sum_{jl} \left\langle b_j b_l \left(Q \cdot H_{jl}^T \cdot Q + L_j \cdot H_{jl}^R \cdot L_l \right) e^{iQ \cdot (\eta_j - \eta_l)} \right\rangle}{\sum_{jl} \left\langle b_j b_l e^{iQ \cdot (\eta_j - \eta_l)} \right\rangle} \quad (2)$$

which is a generalization of the remarkable Akcasu–Gurol (AG) formula (Akcasu and Gurol, 1976) to rotational motion (Bu et al., 2005). Here, b_j is the scattering length of a subunit j , H^T is the translational mobility tensor, and H^R is the rotational mobility tensor. The coordinates of the various subunits (“subunits” can be atoms, beads, or domains), taken relative to the center of friction of the protein, are given by \mathbf{r}_j (note that $\sum \mathbf{r}_j = 0$); $k_B T$ is the usual temperature factor; and $\mathbf{L}_j = \mathbf{r}_j \times \mathbf{Q}$ is the angular momentum vector for each coordinate. The brackets $\langle \rangle$ denote an orientational average over the vector \mathbf{Q} , so that $\langle Q_a Q_b \exp(iQr) \rangle Q^{-2} = (1/3) \delta_{ab} j_0(Qr) + [(1/3) \delta_{ab} - (r_a r_b / r^2)] j_2(Qr)$ can be expressed in terms of the spherical Bessel functions j_n . The translational mobility tensor is illustrated in Fig. 3.

The AG approach described in Eq. (2) is valid for either rigid-bodies or rigid-body subunits connected by soft spring linkers (Bu et al., 2005). The translational mobility tensor H^T is defined by the velocity response $\mathbf{v} = H^T \mathbf{F}$ to an applied force \mathbf{F} . The rotational mobility tensor H^R is defined by the angular velocity response $\boldsymbol{\omega} = H^R \boldsymbol{\tau}$ to an applied torque $\boldsymbol{\tau}$. In practice, the structural coordinates of a protein may be obtained from high-resolution crystallography or NMR or from low-resolution EM, SAXS, or SANS. Comparison of the calculations Eq. (2) to experimental $D_{\text{eff}}(Q)$ thus allows one to test models of the mobility tensors. For example, with a completely flexible body, the rotational diffusion term (involving H^R) is absent.

(Generally speaking, the rotational mobility tensor arises from the consideration of rigid-body constraints, introduced via Lagrange multipliers or by generalized coordinates (Doi and Edwards, 1986)).

Note that the mobility tensors implicitly have two sets of indices. First, there is the index that indicates the specific subunit under consideration, which we denote with Latin letters (j, l, \dots). There is also a second set of indices which indicate the spatial orientation (x, y, z). We will omit this second set of indices for clarity, and use a bold font to indicate vectors. For a rigid-body composed of N identical subunits, the translational mobility tensor H^T is a matrix with N^2 identical 3×3 elements. This must be so, since H^T yields the velocity response of for example, subunits B and C to a force applied to subunit A. If the mobility tensor components H_{AB} and H_{AC} are unequal, the velocity response of B and C will be different, B and C will move apart, and the body will no longer remain rigid. Thus, the mobility tensor provides a direct indication of the existence of internal degrees of freedom (Fig. 8).

It is important to stress a key point in Eq. (2). This formula shows that the effective diffusion constant $D_{\text{eff}}(Q)$ can be calculated if we know the structure of the protein and have a model of the mobility tensor.

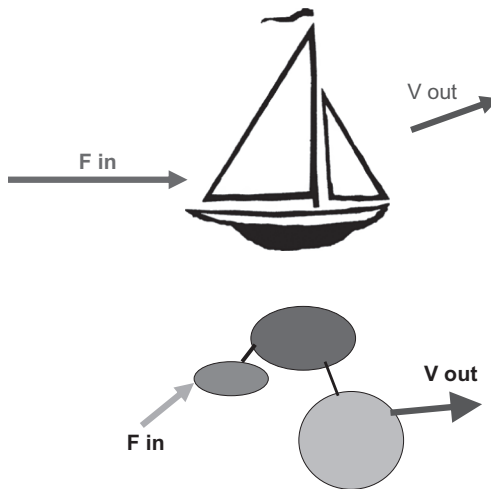


FIG. 8. Translational mobility tensor. The translational mobility tensor gives the velocity response (speed and direction) of a given protein domain to a force applied to itself or to another domain.

In particular, there is no explicit dependence upon force fields or potentials between components of the protein. This is a significant improvement in reliability over complex molecular simulations, which often depend upon numerous parameters that cannot be determined directly. If a complex molecular dynamics simulation yields the wrong answer, it is not immediately obvious how to improve the simulation, as there is no direct connection between experimentally determined quantities and the input parameters.

Our strategy of reducing the NSE data in terms of the AG formula allows a wealth of information to be easily extracted. As another example, note that the diffusion constant for an object is normally defined by the long-time limit of $\langle [r(t) - r(0)]^2 \rangle / 6t \equiv D_\infty$, with $\mathbf{r}(t)$ denoting any vector subunit coordinate of the molecule. Yet, a second definition is commonly used in neutron scattering, that of taking the $Q \rightarrow 0$ limit of the effective diffusion constant, so that $D_{\text{eff}}(Q=0) \equiv D_0$. From the AG result for the first cumulant Eq. (2), we see that for an object composed of N subunits $D_0 = (k_B T \sum_{mn} H_{mn}) / N^2$ (note that the contribution of rotational motion to D_{eff} is zero at $Q=0$ since $\sum_n r_n = 0$). By contrast, an easy result that follows from an elegant paper of Fixman (1983) is that $D_\infty = k_B T / (\sum_{mn} H_{mn}^{-1})$, where H_{mn}^{-1} is the matrix inverse of H_{mn} . Generally $D_\infty \leq D_0$, so that the rate of diffusion of a protein will tend to decrease over time as internal modes damp out. The two diffusion constants are equal if and only if a vector whose components are all equal is an eigenvector of H —in other words, if an identical force applied to all subunits results in an identical velocity response in each subunit. This is of course simply the statement that the object undergoes exact rigid-body motion, typically requiring permutation symmetry among subunits (like the vertices of a Platonic solid). *Thus, the decrease of D with time can provide another signature of internal motion.*

In contrast to NSE spectroscopy, other neutron-scattering techniques (e.g., time-of-flight or backscattering) have significantly less precision in determining energy transfer (Higgins and Benoit, 1994), and so typically measure only the dynamic form factor $S(Q, \omega) = \int e^{i\omega t} I(Q, t) dt$, which then must be fit to mathematical functions or Fourier transformed numerically. However, in all cases, the important quantity to determine is the effective diffusion constant $D_{\text{eff}}(Q)$ [or equivalently $\Gamma(Q) \equiv Q^2 D(Q)$] as a function of Q . This directly yields the desired information about the degree and nature of internal protein dynamics.

These concepts can be illustrated by applying them to study bulk properties of a simple protein. Earlier, we reported a neutron-scattering study of the nanosecond and picosecond dynamics of native and denatured alpha-lactalbumin (Bu et al., 2001). The quasielastic-scattering intensity shows that there are alpha-helical structure and tertiary-like side-chain interactions fluctuating on subnanosecond timescales under extremely denaturing conditions and in the absence of disulfide bonds. The nanosecond dynamics of the native and the denatured proteins was found to have three dynamic regimes (Fig. 9). When $0.05 < Q < 0.5 \text{ \AA}^{-1}$ (where the scattering vector, Q , is inversely proportional to the length scale), the decay rate, $\Gamma(Q)$, shows a power law relationship, with $\Gamma(Q)$ proportional to $Q^{(2.42 \pm 0.08)}$, that is analogous to the dynamic behavior of a random coil. However, when $0.5 < Q < 1.0 \text{ \AA}^{-1}$, the decay rate exhibits a $\Gamma(Q)$ proportional to $Q^{(1.0 \pm 0.2)}$ relationship. The effective diffusion constant of the protein therefore decreases with increasing Q , a striking dynamic behavior that is not found in any chain-like macromolecule.

These results stand in dramatic contrast to the results obtained in the canonical models of polymer dynamics, which we review here (Doi and Edwards, 1986). The main models of polymer dynamics can be summarized by the Rouse model (Ferrand et al., 1993) and the Zimm model (Fixman, 1983). In the Rouse model, one considers a polymer whose dynamics are given by Brownian motion. The polymer is simply a chain of beads that interact via harmonic oscillator springs, with each bead on the chain interacting only with the beads behind and ahead of it. Hydrodynamic interactions and repulsive interactions between the beads are ignored. The Rouse model can be shown to yield a result for the decay rate $\Gamma(Q) \approx Q^4$ when Q is large enough that internal motion can be seen. The Zimm model is mathematically more elaborate, and also includes a crude approximation to the hydrodynamic contributions to the mobility tensor, as estimated via the Navier-Stokes equation. In the Zimm model, one arrives at the large Q result $\Gamma(Q) \approx Q^3$. (Both of these results can also be easily derived by using scaling arguments originally due to De Gennes (Mi et al., 1994.) Finally, we note that for small Q , $\Gamma(Q) \approx Q^2$ (the limit of overall rigid-body diffusion).

We suggested that this unusual internal protein dynamics is due to the presence of a strongly attractive force and collective conformational fluctuations in both the native and the denatured states of the protein. Above $Q > 1.0 \text{ \AA}^{-1}$ is a regime that displays the local dynamic behavior of individual

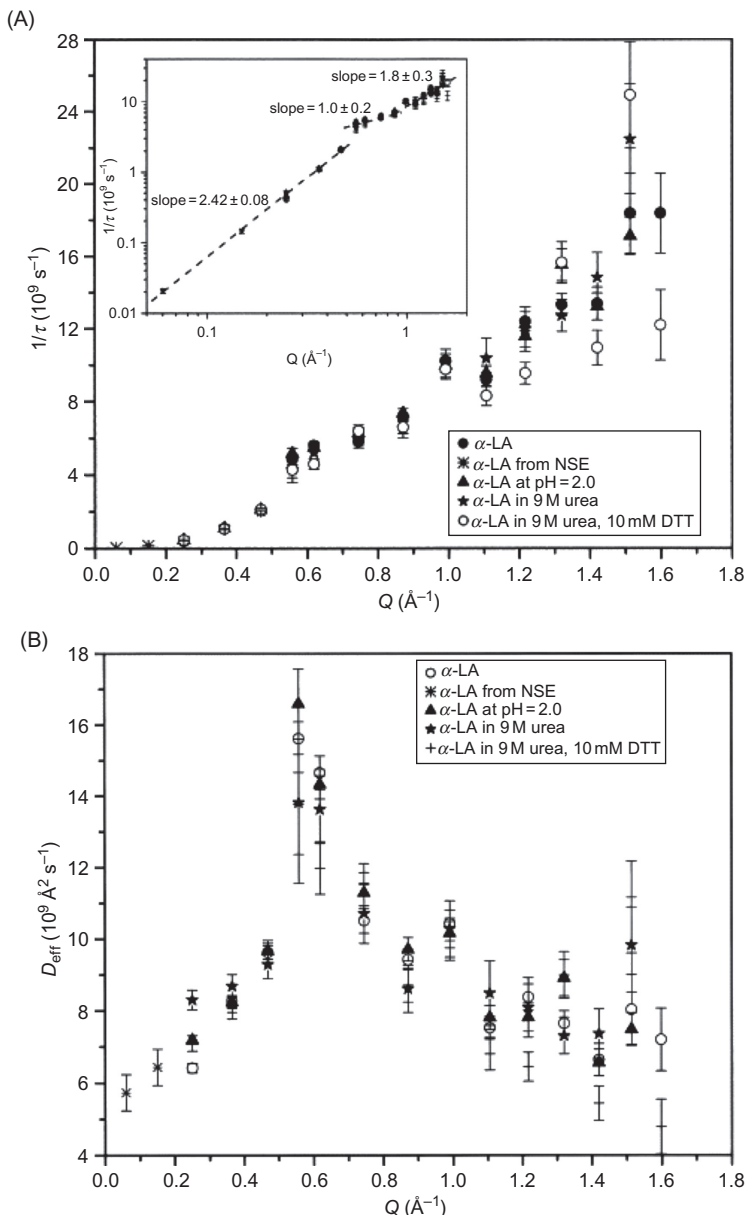


FIG. 9. (A) The nanosecond decay rate (or $1/\tau$) as a function of Q . (B) The effective diffusion constant $D_{\text{eff}} = \Gamma/hQ^2$ of the native protein and the denatured proteins as a function of the scattering vector.

residues, with $\Gamma(Q)$ proportional to $Q^{(1.8 \pm 0.3)}$ indicating free-body diffusion. Our results provide a dynamic view of the native-like topology established in the early stages of protein folding, and yield a sense of the unusual bulk dynamics properties of proteins. In particular, this result suggests that the conformational entropy in protein matter is significantly lower in an unfolded protein than in a random coil. This dynamic behavior is reminiscent of collective density fluctuations found in fluids, suggesting the existence of strongly nonlocal, attractive forces within proteins.

We now return to the general problem of understanding long-range protein dynamics via Eq. (2). The rotational mobility tensor H^R for the entire protein is derived by evaluating the torque by summing over all subunits m :

$$\begin{aligned}\boldsymbol{\tau} &= (H^R)^{-1} \boldsymbol{\omega} = \sum_m (\mathbf{r}_m \times \mathbf{F}_m) \\ \mathbf{F}_m &= \sum_n (N^2 H^T)^{-1}_{mn} \mathbf{v}_n = \sum_n (N^2 H^T)^{-1}_{mn} (\boldsymbol{\omega} \times \mathbf{r}_n)\end{aligned}\quad (3)$$

Equation (3) generally yields the simple estimate $D_{\text{eff}}(Q \rightarrow \infty) = 2D_{\text{eff}}(Q=0)$ for *rigid-bodies composed of identical (e.g., nondeuterated) point subunits*. We adopt the simplifying assumption that the three principal spatial components of the translational mobility tensor for each subunit are equal to $ND_0/(k_B T) = 1/\zeta$ with ζ the friction constant of a subunit and D_0 the measured diffusion constant of the protein. Then $\mathbf{F}_n = \zeta \mathbf{v}_n = \zeta (\boldsymbol{\omega} \times \mathbf{r}_n)$. Thus, Eq. (3) yields the rotational mobility tensor H^R via a straightforward inversion of a 3×3 matrix. A fair estimate of the rigid-body $D_{\text{eff}}(Q)$ measured by NSE can therefore be made using only the coordinates and diffusion constant D_0 of the system. We now explain our reasoning.

We take the rigid-body as consisting of a collection of N identical beads. The case of a continuous solid can be reached by an appropriate limit if desired. First, we note that for a rigid-body, the rotational and translational mobility tensors are simply 3×3 matrices, identical for each bead. This must be so, since otherwise a force applied to a given bead would result in different resultant velocities for other beads, and the body would not remain rigid. Thus, we see that the mobility tensor defines and characterizes internal motion for a body. We also make the simple observation that $\exp(i\mathbf{Q}\mathbf{r})$ is one for all values of the vector \mathbf{r} at zero \mathbf{Q} , and that, as Q increases without bound, this quantity is one when r is zero and equals zero otherwise. The remainder of our analysis begins with the Akcasu-Gurol (AG) formula Eq. (2). We shall adopt the convention that the indices that identify a given bead will be labeled with Latin subscripts (m, n, \dots) while spatial indices

(x,y,z) will be indicated with Greek symbols ($\alpha, \beta, \gamma, \dots$), and are typically omitted for clarity, with vector quantities indicated by bold script. We note that at $Q=0$, the contribution to $D_{\text{eff}}(Q)$ from translational diffusion is $D_{\text{eff}}^T(Q=0) = k_B T (\sum_{mn} H_{mn}^T) / N^2$, while at infinite Q this contribution becomes $D_{\text{eff}}^T(Q \rightarrow \infty) = k_B T (\sum_{nn} H_{nn}^T) / N = k_B T \text{Tr}(H^T) / N$. We point out for later use that for a rigid-body, $D_{\text{eff}}^T(Q=0) = D_{\text{eff}}^T(Q \rightarrow \infty)$ since H^T is independent of n . By contrast, $D_{\text{eff}}^R(Q)$, the contribution to $D_{\text{eff}}(Q)$ from rotational diffusion, is zero at $Q=0$, since $\sum_n \mathbf{r}_n = 0$ by definition of our coordinate system. Of course, $D_{\text{eff}}(Q) = D_{\text{eff}}^T(Q) + D_{\text{eff}}^R(Q)$. The calculation of the contribution of rotational diffusion at large Q is slightly more involved, and will now be considered in detail.

The contributions to rotational diffusion are normally evaluated using the usual methods for systems involving rigid constraints, such as Lagrange multipliers or generalized coordinates (see Doi and Edwards, 1986, Section 3.8). The following course is simpler and suffices here. The angular velocity vector of the rigid object is given by $\boldsymbol{\omega} = H^R \boldsymbol{\tau}$, with the torque $\boldsymbol{\tau} = \sum_n \mathbf{r}_n \times \mathbf{F}_n$. The vector force \mathbf{F}_n on bead n is given in terms of the velocity \mathbf{v}_n and overall angular velocity $\boldsymbol{\omega}$ by Eq. (3). Thus for an arbitrary three-component vector $\boldsymbol{\omega}$ following Eq. (3)

$$\boldsymbol{\omega} = H^R \sum_{mn} r_m \times (N^2 H^T)^{-1} (\boldsymbol{\omega} \times \mathbf{r}_n) \quad (4)$$

We note that Eq. (4) is of the form $\boldsymbol{\omega} = M \boldsymbol{\omega}$ for an arbitrary vector $\boldsymbol{\omega}$, implying that M is the identity matrix. It immediately follows that the 3×3 matrix H^R can be evaluated by an inversion of a 3×3 matrix calculated by summing over bead coordinates n . *The rotational mobility tensor is thus entirely determined by the translational mobility tensor.* In the simplified case (adopted in this work), where the x , y , and z principal components of the translational mobility tensor H^T are all set equal to a friction constant $1/\zeta$ (see discussion surrounding Eq. (3)), a compact formula arises in terms of a 3×3 matrix inverse, arising from the protein diffusion constant D_0 (measured by NMR) and the N structural coordinates of the protein (defined so that $\sum_n r_n = 0$):

$$H_{\alpha\beta}^R = N(D_0/k_B T) \left[\sum_n (\delta_{\alpha\beta} r_n^2 - r_{\alpha} r_{\beta}) \right]^{-1} \quad (5)$$

To complete the proof that $D_{\text{eff}}(Q \rightarrow \infty) = 2D_{\text{eff}}(Q=0)$, we now use the fact that $\boldsymbol{\omega}$ is arbitrary, set $\boldsymbol{\omega} = H^T \mathbf{Q}$ in Eq. (4), contract the remaining vector

index on the left-hand side with \mathbf{Q} , and perform an average $\langle \dots \rangle$ over the orientation of \mathbf{Q} :

$$\begin{aligned} D_{\text{eff}}^T(Q \rightarrow \infty) &= k_B T \sum_n \langle \mathbf{Q} H^T \mathbf{Q} \rangle / (NQ^2) \\ &= k_B T \sum_n \langle (\mathbf{Q} \times \mathbf{r}_n) H^R (\mathbf{Q} \times \mathbf{r}_n) \rangle / (NQ^2) \\ &= D_{\text{eff}}^R(Q \rightarrow \infty) \end{aligned} \quad (6)$$

from which we see that at large Q the translational and rotational contributions to the AG formula are identical, so $D_{\text{eff}}(Q=0) = D_{\text{eff}}^T(Q=0) = D_{\text{eff}}^R(Q \rightarrow \infty) = D_{\text{eff}}^R(Q \rightarrow \infty)$. Since $D_{\text{eff}}(Q) = D_{\text{eff}}^T(Q) + D_{\text{eff}}^R(Q)$ this completes the proof.

We will also demonstrate that in general one *only* has the bound $D_{\text{eff}}(Q \rightarrow \infty) \geq D_{\text{eff}}(Q=0)$. We consider a system with no rigid constraints, so there is only one mobility tensor H . We also omit spatial indices in the interests of clarity.

Note that the second law of thermodynamics assures us that the power dissipated by a system is generally nonnegative (Doi and Edwards, 1986, Eq. (3.18)), therefore

$$\sum_n \mathbf{v}_n \mathbf{F}_n = \sum_{mn} \mathbf{F}_m H_{mn} \mathbf{F}_n \geq 0 \quad (7)$$

for any set of applied forces \mathbf{F} , and therefore the mobility tensor is positive semidefinite (has no negative eigenvalues). If we choose \mathbf{F} to have only two nonzero components, $\mathbf{F}_m = 1$ and $\mathbf{F}_n = -1$, we see that Eq. (7) implies that H is dominated by its diagonal elements:

$$H_{mm} + H_{nn} \geq H_{mn} + H_{nm} \quad (8)$$

We now sum over all indices m and n , and note that Eq. (8) implies

$$D_{\text{eff}}(Q \rightarrow \infty) = k_B T \text{Tr}(H)/N \geq k_B T \sum_{mn} H_{mn}/N^2 = D_{\text{eff}}(Q=0) \quad (9)$$

The inequality approaches the equality $D_{\text{eff}}(Q \rightarrow \infty) = D_{\text{eff}}(Q=0)$ when all elements of H are equal (the delicate singular limit of a stiff but still flexible body, discussed in Bu et al. (2005)). In the other extreme limit, when the mobility tensor is entirely diagonal (the limit of noninteracting beads in a flexible system) we have

$$D_{\text{eff}}(Q \rightarrow \infty) = N D_{\text{eff}}(Q=0) \quad (10)$$

For a system with an infinite number N of subunits, $D_{\text{eff}}(Q \rightarrow \infty)$ thus increases without bound in the case of a diagonal mobility tensor (cf. the

Rouse model of polymers). Thus we see that the uniform rigid body result $D_{\text{eff}}(Q \rightarrow \infty) = 2 D_{\text{eff}}(Q=0)$ is quite unusual. In the above calculation of H^R , as well as below, we assume that the x , y , and z diagonal components of H^T are equal for each subunit and are the only nonzero components. In general, of course, both the rotational and translational mobility tensors have different values for each of the three principal axes, so that there are six independent qualities for each domain. In a multidomain complex like NHERF1 bound to the FERM domain of ezrin, there are generally at least 24 independent quantities for the mobility tensor (three translational plus three rotational for each of the four subunits). These quantities are difficult to evaluate to the precision required to compare with NSE data. Programs such as HYDROPRO utilize continuum Navier-Stokes equations to estimate the mobility tensor components from structural coordinates (Garcia De La Torre et al., 2000), but a continuum approximation is insufficiently accurate for our purposes because many structural features of a protein are of the same size as water molecules. By contrast, our simple approach requires neither complicated molecular dynamics simulations nor Navier-Stokes hydrodynamics. The effects of scattering length inhomogeneity can also be neglected as neutron scattering occurs mostly from hydrogen atoms.

For an object with internal domain motion, comparing the calculated $D_{\text{eff}}(Q)$ with data allows one to extract the relative degree of dynamic coupling between the various components of the system, for this dynamic coupling is defined by the mobility tensor. For example, a rigid two-domain system will be described by a mobility tensor

$$H = H_0 \begin{pmatrix} 1 & 1 \\ 1 & 1 \end{pmatrix} \quad (11a)$$

with all elements of the tensor equal, and yields [via Eq. (2)] the simple result that the translational contribution to the effective diffusion constant is given by $D_{\text{eff}}^T(Q) = k_B T H_0$, independent of Q . By contrast, a two-domain system with internal motion will possess a mobility tensor

$$H = \begin{pmatrix} H_1 & 0 \\ 0 & H_2 \end{pmatrix} \quad (11b)$$

in principal coordinates. Thus, the application of equal forces to the two domains will result in their having different velocities, revealing internal motion. For the case where there is one internal translational mode

between subunits 1 and 2 with $D_1 = k_B T H_1$ and $D_2 = k_B T H_2$ (Bu et al., 2005), the translational contribution to the effective diffusion constant is

$$D_{\text{eff}}^T(Q) = \frac{D_1 S_1(Q) + D_2 S_2(Q)}{S(Q)} \quad (11c)$$

Here, $S_1(Q)$ and $S_2(Q)$ are the form factors of the separate individual protein domains, while $S(Q)$ is the form factor of the entire protein. Orientational averages are performed, so that for example, $S(Q) = \sum_j S_j(Q)$; and $S(Q)$ is normalized so that $S(0) = N^2$.

Rotational diffusion will introduce additional contributions to the numerator, as per Eq. (2). The calculations we perform here consist of rigid-body motion (including both translational and rotational motion), and an internal translational mode as per Eqs. (11b) and (11c). We stress that, in principle, it is possible to include the effects of arbitrary translational and rotational internal motion in the calculation (Bu et al., 2005). Therefore, the combination of NSE and first cumulant analysis allows one to test complex models of the mobility tensors of the system, and extract dynamical information about the internal motion of the protein.

C. Dynamic Propagation of Allosteric Signals by Nanoscale Protein Motion

The virtue of the above simple approach can be seen by comparing the NSE data $D_{\text{eff}}(Q)$ for unbound NHERF1 with the rigid-body calculation using Eqs. (2), (3), and (11a) (Farago et al., 2010). The rigid-body calculation uses as input only the translational diffusion coefficient D_0 of NHERF1 obtained from pulsed-field gradient (PFG) NMR, and the “dummy atom” structural coordinates (Svergun, 1999) reconstructed from SAXS (Li et al., 2007a, 2009). Figure 10B shows that the calculated rigid-body $D_{\text{eff}}(Q)$ fits the NSE experimental data quite well, except at high Q where the experimental $D_{\text{eff}}(Q)$ is slightly smaller than the computed values (Farago et al., 2010). This is possibly due to fine structural differences from that represented by the coordinates reconstructed from SAXS. Thus, NHERF1 behaves essentially as a rigid-body on the time and length scales detected by our NSE experiment. The rotational diffusion relaxation time $1/H_0^R$ can be estimated (via Eq. (3)) to be about 1000 ns. The Fourier time-window employed in our NSE experiments is between 0.3 and 200 ns. Thus rotational diffusion is present in the time-window of the NSE experiments.

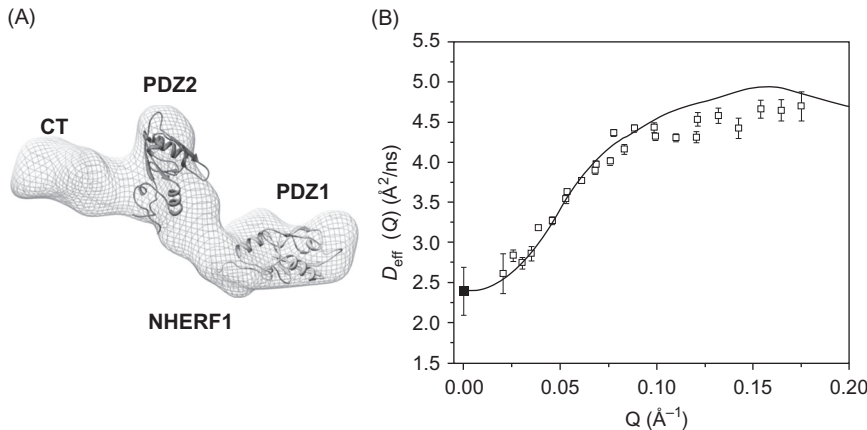


FIG. 10. NHERF1 alone can be described by a rigid-body model. (A) The 3D shape of NHERF1 reconstructed from SAXS (Li et al., 2009) using the *ab initio* program DAMMIN (Svergun, 1999). The known high-resolution structures of the PDZ1 (PDB code: 1I92) and PDZ2 (PDB code: 2KJD) domains are docked into the 3D shape, using UCSF chimera (Pettersen et al., 2004). EBD, which overlaps with the last 13 amino acid residues that interact with PDZ2 is not marked in the graph. (B) Comparing the experimental NSE $D_{\text{eff}}(Q)$ of NHERF1 (black open square) with the rigid-body calculation (black solid line). The overall translational diffusion constant D_0 (filled black square) at $Q=0 \text{ \AA}^{-1}$ is $D_0=2.4 \text{ \AA}^2/\text{ns}$ from pulsed-field gradient (PFG) NMR measurements.

As one might expect from the *unbound* NHERF1, the salient features of protein domain motion, as viewed by NSE, can be understood in terms of simple models. We next use this direct approach and construct models of increasing sophistication to demonstrate domain motion in the complex of NHERF1 bound to the FERM domain of ezrin. Because our approach depends on few assumptions, it is subject to less unquantifiable uncertainty than a large scale multiparameter fit or molecular dynamics simulation.

We have performed NSE experiments on two types of complexes of NHERF1 bound to the FERM domain of ezrin. One is the hydrogenated NHERF1 bound to hydrogenated FERM (NHERF1·^hFERM), and the other is hydrogenated NHERF1 bound to deuterium labeled FERM (NHERF1·^dFERM). We then performed a series of computations of $D_{\text{eff}}(Q)$ for both the deuterated and hydrogenated complexes. When calculating $D_{\text{eff}}(Q)$ for the NHERF1·^dFERM complex, the scattering from the deuterated component is treated as “invisible” in Eq. (2) because the neutron-scattering length density of the deuterated component contrast matches that of the D_2O buffer background.

We have previously shown that deuteration does not cause aggregation or conformational changes in the NHERF1-FERM complex (Li et al., 2009). At low Reynolds number, the dynamics of a protein should not depend upon its mass, but rather upon its size (Howard, 2001). Thus, the dynamics of the deuterated complex can be treated as similar to that of the hydrogenated complex. The PFG NMR results show that NHERF1^{·h}FERM and NHERF1^{·d}FERM complexes have very similar translational diffusion constants, in support of this assertion (Fig. 11B). In our calculations, we thus always

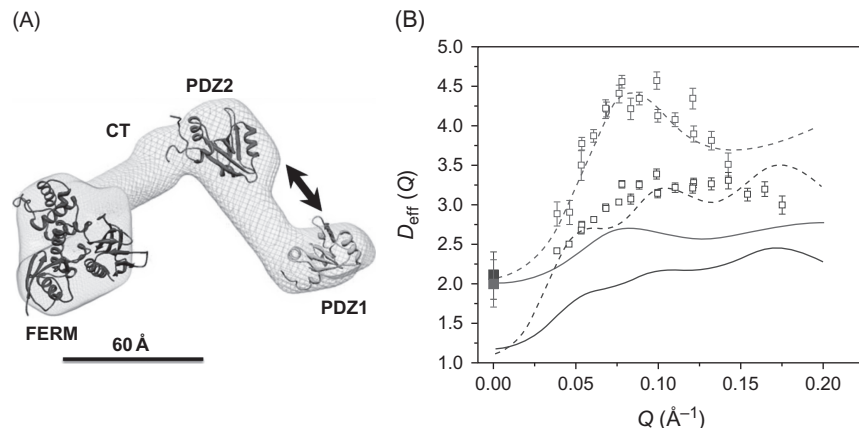


FIG. 11. (A) A model representing domain motion between PDZ1 and PDZ2 in the complex. The 3D shape of the complex is reconstructed from SANS (Li et al., 2009). The known high-resolution structure fragments of PDZ1, PDZ2, and ezrin FERM domain (PDB code: 1NI2) are docked into the envelope using UCSF chimera (Pettersen et al., 2004). The arrows represent translational motion between PDZ1 and PDZ2. A length scale bar of 60 Å is shown. (B) Comparing experimental $D_{\text{eff}}(Q)$ of NHERF1-FERM with calculations incorporating interdomain motion between PDZ1 and PDZ2. The calculations were performed using the coordinates of the docked high-resolution structures of different domains. The calculations were performed with only one adjustable parameter H^T for the domain motion model of both the deuterated and the hydrogenated complexes. Open blue square is the NSE data from hydrogenated complex. Open red square is NSE data from hydrogenated NHERF1 in complex with deuterated FERM domain. Solid blue square and solid red square are the self-diffusion constants D_0 of the hydrogenated and the deuterated complexes, respectively, obtained from PFG NMR. The calculated curves are shown for NHERF1^{·d}FERM (solid red line for rigid-body model and dashed red line for model incorporating domain motion) and NHERF1^{·h}FERM (solid blue line for rigid-body model and dashed blue line for incorporating domain motion). The comparisons suggest that deuteration of the FERM domain amplifies the effects of protein internal motions detected by NSE. (See color plate 4).

impose the constraint that the dynamics (and therefore the mobility tensors) of the hydrogenated and deuterated components is the same. As we show below, this provides a significant and essential constraint.

Using the same approach applied to NHERF1, we have first performed a rigid-body calculation of $D_{\text{eff}}(Q)$ for the deuterated NHERF1-^dFERM complex. The structural coordinates of the complex are the “dummy atoms” (Petoukhov and Svergun, 2006) reconstructed from SANS data (Li et al., 2009) (shown in Fig. 11A), and the one constraint parameter $D_{\text{eff}}(Q=0)$ is the self-diffusion constant D_0 for this deuterated complex, taken from PFG NMR. We then use the same approach and parameter to compute the $D_{\text{eff}}(Q)$ of the hydrogenated NHERF1-^hFERM complex. As shown in Fig. 11B, the agreement between the experimental data and *rigid-body* calculations is poor for both the NHERF1-^dFERM and the NHERF1-^hFERM complex.

We argue that the difference between the experimental NSE results and dummy atom rigid-body calculations arises because of the internal motion of the protein. This internal motion produces various effects: the first way in which internal motion manifests itself is through the fact that the mobility tensor associated with a protein with internal motion is different than the mobility tensor for a rigid-body. This was discussed above (see Eqs. (11a)–(11c)).

Second, it is essential to note that the evaluation of Eq. (2) implicitly requires an average over a distribution of particle densities. For the purposes of this calculation, the SAXS/SANS dummy atom structural data may be an accurate representation for a rigid-body, but will be inaccurate for a protein with a significant degree of internal dynamics. This is because *ab initio* programs utilized for shape reconstruction from SANS or SAXS data typically produce an envelope of the calculated structure, in which the density inside the envelope is assumed constant. In a highly mobile object, the reconstructed shape may thus be a poor representation of the fluctuating structures. Thus, for example, if the linker regions between domains are highly mobile, the size of the linker regions may be overestimated, and the dummy atom shape reconstruction will not be a good representation of the entire protein. We speculate that the disagreement between the experimental NSE data and that computed from the SANS reconstructed shape model (Fig. 11B) is partly due to this variation of density within the reconstructed shape.

Thus, in the following, we construct two models incorporating these internal motion effects in order to understand the discrepancy between the

calculations and experimental data. We first present a more detailed rigid-body model, in which the known high-resolution structural fragments of the PDZ1, PDZ2CT, and the FERM domains are docked into the 3D shapes reconstructed from SANS (Fig. 11A) using the software package UCSF Chimera (Pettersen et al., 2004). This “docked” model therefore incorporates a crude form of density variation within the complex, by ignoring the density of the linker regions. The mobility tensor for this first model is taken to be that for a rigid-body. It will be seen that this density variation alone does not yield a good comparison with the NSE data. We therefore construct a second “docked” model in which the mobility tensor used is that for interdomain motion between the two PDZ domains. It will be seen that the second model produces a sizeable improvement in explaining the data.

When calculating the $D_{\text{eff}}(Q)$ using the docked coordinates, the rigid-body mobility tensor docked calculations again provide poor fits to the NSE data for both the hydrogenated and deuterated complexes. The comparison thus suggests that NHERF1·^hFERM and NHERF1·^dFERM do not behave as rigid-bodies on the length scales and timescales of the NSE experiments. This observation is supported by our previous SANS and NMR structural studies that find large conformational changes in NHERF1 upon binding to FERM (Li et al., 2009; Bhattacharya et al., 2010). In particular, the region that links PDZ1 and PDZ2 becomes more extended, and the CT region of NHERF1 becomes largely unfolded upon binding to FERM. Thus, structural fluctuations in the complexes can become significant in the complex on the length scales and timescales of the NSE experiments.

We next incorporate interdomain motion in the mobility tensor for the NHERF1·^dFERM and NHERF1·^hFERM complexes in our calculation. To compute $D_{\text{eff}}(Q)$ with domain motion using Eqs. (2)–(4), we use the coordinates of the docked model (Fig. 11A), and assume translational interdomain motion between PDZ1 and PDZ2 (Eq. (11b)). Here we perform the calculation, as always, with only one adjustable parameter, the translational diffusion constant for each atom. Again, this parameter is adjusted so that $D_{\text{eff}}(Q)$ for the deuterated complex agrees with the value measured by PFG NMR. As with the above calculations, we use this same parameter for both the deuterated and hydrogenated complexes. When performing the calculations, the rotational contributions to diffusion (Eq. (3)) are taken to be the same as for the rigid-body docked model calculation. The difference with the previous docked calculation is thus solely that in this second docked model calculation we employ the mobility tensor for a protein with an internal mode between

the PDZ1 and PDZ2 domains, rather than a rigid-body mobility tensor. After incorporating interdomain motion between PDZ1 and PDZ2 in the NHERF1.^dFERM complex, the calculated $D_{\text{eff}}(Q)$ with internal motion agrees well the NSE results (Fig. 11B). In particular, the docked calculation with the internal mode mobility tensor generates a peak at a Q value of 0.07 \AA^{-1} in Fig. 3D, which agrees well with the NSE results. For the NHERF1.^bFERM complex, there is also better agreement between the experimental data and the calculation after incorporating interdomain motion between PDZ1 and PDZ2 (Fig. 11B). Nevertheless, we note that, for the docked NHERF1.^bFERM complex, the computed D_0 at $Q=0$ is not close to the experimental values from PFG NMR measurement. As pointed out above, we attribute this discrepancy to large conformational fluctuations in the CT–FERM region caused by the unfolding of the CT domain upon binding to FERM (Bhattacharya et al., 2010), which cannot be represented by a single reconstructed SANS structure shown in Fig. 3A. Such complications are minimal in the NHERF1.^dFERM complex because the deuterated ^dFERM is “invisible” to neutrons. Future experiments could use selective deuteration of other portions of the complex in order to highlight the motions of PDZ2–CT–FERM domains for NSE study.

D. A Simple Four-Point Model Describes Domain Motion

The simple calculations we presented above require only the structural coordinates and a single constraint (the diffusion constant at $Q=0 \text{ \AA}^{-1}$ for the deuterated complex, measured independently by PFG NMR) to generate the computed $D_{\text{eff}}(Q)$. It is possible to argue however that the structural coordinates are insufficiently accurate to explain the NSE data, or that some coincidental artifact produces the peak at 0.07 \AA^{-1} that implies internal motion. We therefore introduce an even more simplified model that yields the same effect, and serves to explain its origin. The simplified model is taken by extracting four points that represent the coordinates of the center-of-mass of domains obtained from the SANS data of the NHERF1–FERM complex. These points form a triangle model as shown in Fig. 12A with the distances FERM–PDZ2 = 80 \AA , PDZ2–PDZ1 = 59 \AA , and FERM–PDZ1 = 110 \AA . The CT domain is taken as being halfway between the FERM and PDZ2 domains (Fig. 12A). We include the point representing the FERM domain with a weight factor of 3 to account for its larger size relative to the other

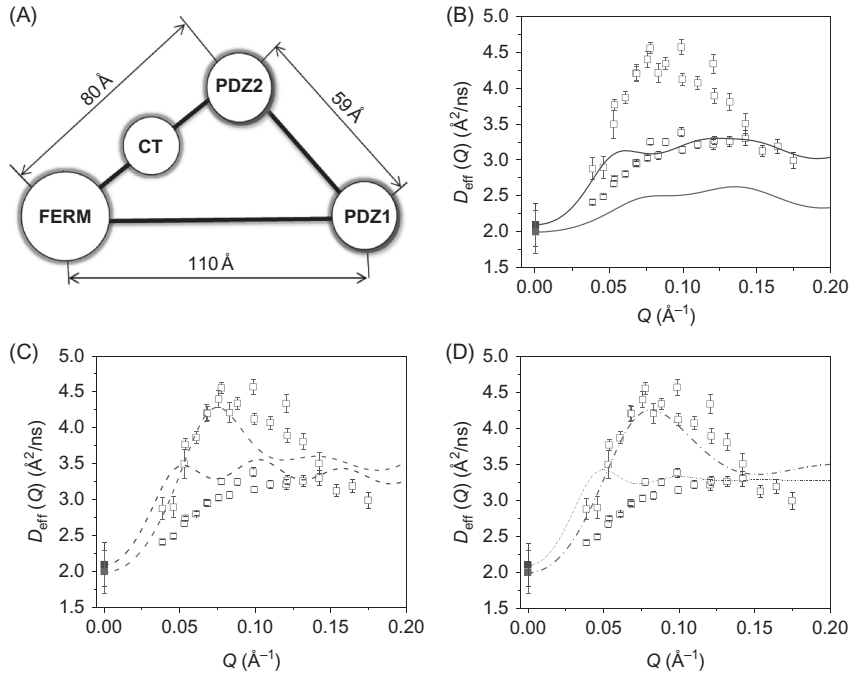


FIG. 12. A simple four-point model can well describe domain motion in the complex. (A) The four-point model represents the NHERF1-FERM complex, with the centers of PDZ1, PDZ2, CT, and FERM domain taken from Fig. 3A. (B) Comparing the experimental NSE data with the four-point rigid-body calculations for NHERF1-^hFERM (blue open squares are the experimental data and blue solid line is the calculated data) and for NHERF1-^dFERM (red open squares are experimental data and red solid line is the calculated data). D_0 of NHERF1-^dFERM (solid red squares) and NHERF1-^dFERM (solid blue squares) from PFG NMR are shown. (C) Comparing the experimental data with calculations assuming interdomain motion between PDZ1 and PDZ2 in NHERF1-^dFERM (red dash line) and NHERF1-^hFERM (blue dash line). The experimental symbols are the same as in (B). (D) Comparing the experimental data with calculations incorporating interdomain motion between PDZ1 and PDZ2, as well as assuming finite size form factor of spheres of 20 Å radius for the FERM domain and for both PDZ domains in NHERF1-^dFERM (red dash dot line) and in NHERF1-^hFERM (blue dash dot line). (See color plate 5).

domains. Because it is possible to obtain the center-of-mass distances between the domains with confidence even with low resolution SAXS or SANS data, this model possesses fewer uncertainties than a model based upon the molecular shape.

We first present the calculation of the four-point model representing the deuterated NHERF1^dFERM and hydrogenated NHERF1^hFERM complexes. The calculation has one adjustable parameter, the domain translational diffusion constant D_{domain}^T , which is chosen to yield the correct value for the diffusion constant D_0 of the deuterated complex (as measured by PFG NMR). For the model with internal motion, the domain diffusion constant is taken the same for the FERM, the CT, and the two PDZ domains. We use $D_{\text{domain}}^T = 2.9 \times 10^{-7} \text{ cm}^2/\text{s}$ for the domain diffusion constant for both the deuterated and hydrogenated systems. Note that the diffusion constant D^T for the individual domains is larger than that for the complex, as expected. Interestingly enough, the diffusion constant for the hydrogenated complex ($2.1 \times 10^{-7} \text{ cm}^2/\text{s}$) is estimated correctly by this procedure, and is thus an output. The rotational diffusion constant is then estimated using the Stokes formula for a sphere $D_{\text{domain}}^R = (3/4)D_{\text{domain}}^T/R_S^2$, with the Stokes-Einstein radius $R_S = k_B T / (6\pi\eta D_{\text{domain}}^T)$ and is taken to be identical for all domains. Such an estimate has been shown to be valid for a number of proteins (Yao et al., 2008).

In our four-point calculation, we assume that the PDZ1 domain is a separate subunit, and so there is a degree of internal motion in the protein, appearing as *translational* mode between PDZ1 and PDZ2. The translational mobility tensor for the PDZ1 domain is thus a simple constant, while the FERM, CT, and PDZ2 domains are treated as rigid subunits and thus their translational mobility tensor is a 3×3 matrix (whose xyz elements are all equal). The rotational mobility tensor is a 4×4 matrix, taken as the same as a rigid-body. Thus, we see that the topological dynamic connectivity of the mobility tensors defines the Q dependence of the effective diffusion constant, while their numerical values largely determine only its overall scale. It is, of course, the connectivity that defines the degree and nature of protein internal motion.

Figure 4B compares the experimental NSE data with the calculated $D_{\text{eff}}(Q)$ from the rigid four-point model for the hydrogenated and the partially deuterated complexes. Figure 12C is the $D_{\text{eff}}(Q)$ of the four-point model incorporating internal domain motion between PDZ1 and the rest of the complex. After incorporating internal motion, the overall $D_{\text{eff}}(Q)$ from the four-point model agrees well with the experimental data for both the partially deuterated and the hydrogenated complexes. There are however some oscillations remaining, for we have approximated the domains as point objects.

The comparison between calculation and experimental data improves considerably after including the form factor of a 20 Å radius sphere for the FERM domain and both PDZ domains in the calculation (Fig. 12D). Thus, the NSE data is better represented by the four-point model that includes PDZ1–PDZ2 oscillatory motion than by a model that assumes the complex as a rigid-body. Further improvement likely requires the use of methods of evaluating the mobility tensors for proteins with high accuracy.

Moreover, from the four-point model calculations, we note that $D_{\text{eff}}(Q)$ for the hydrogenated rigid complex and the hydrogenated complex with internal motion are nearly indistinguishable (Fig. 13A). For the deuterated complex, $D_{\text{eff}}(Q)$ obtained from the interdomain motion model is

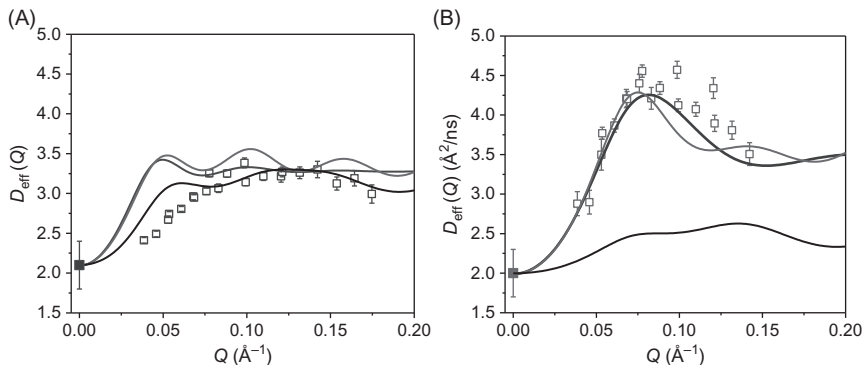


FIG. 13. For the hydrogenated NHERF1^hFERM complex, the difference in $D_{\text{eff}}(Q)$ between the rigid-body model and domain-motion models is very small, but is significantly increased in the deuterated complex. (A) Comparing the rigid-body calculation with the domain-motion calculation in the four-point model in the hydrogenated NHERF1^hFERM complex. NSE data from the NHERF1^hFERM (blue open squares), the four-point rigid-body model (black line), four-point model incorporating domain motion between PDZ1 and PDZ2 (red line), four-point model incorporating domain motion between PDZ1 and PDZ2 and finite size form factor of 20 Å radius for the FERM domain, PDZ1 and PDZ2 (blue line). D_0 at $Q=0$ Å⁻¹ as measured from PFG NMR is shown in blue solid square. (B) Comparing the rigid-body calculation with the domain-motion calculation in the four-point model in the deuterated NHERF1^dFERM complex. NSE data from the NHERF1^dFERM (red open squares), the four-point rigid-body model (black line), four-point model incorporating domain motion between PDZ1 and PDZ2 (red line), four-point model incorporating domain motion between PDZ1 and PDZ2 and finite size form factor of 20 Å radius for the FERM domain, PDZ1 and PDZ2 (blue line). D_0 at $Q=0$ Å⁻¹ as measured from PFG NMR is shown in red solid square. (See color plate 6).

significantly different from that of the rigid-body model (Fig. 13B). This can be explained as due to the relatively large contribution to Eq. (2) of the effects of rotational diffusion of the overall object, which dominates and obscures the effects of internal motion when no deuteration is performed. For the partially deuterated complex, both the docked domain calculation (Fig. 11) and the four-point model (Fig. 12B–D) show that $D_{\text{eff}}(Q)$ of the rigid-body complex is significantly different from that of the complex with internal domain motion. These analyses demonstrate that deuterium labeling of a domain in a protein or in a protein complex significantly amplifies the effects of internal motion detected by NSE. Our model calculations (Fig. 13A and B) suggest that deuterium labeling a domain can mask a portion of the form factor, and, as a result, highlight the contribution of the terms of internal domain motion in Eq. (2). Thus, we propose that future NSE experiments will benefit by utilizing the strategy of selective deuteration to highlight the domain motion of interest.

Multidomain proteins and protein complexes are complicated systems containing thousands of atoms, and providing precise answers to questions can be done, if at all, by large-scale simulations. We demonstrate in this chapter that the NSE results can be explained by a detailed docked model, as well by a highly simplified four-point model that is independent of the details of the structural model. By doing so, we have systematically reduced the relevant assumptions, making the results of our calculations progressively more certain.

E. The Importance of NSE and a Plan for the Future

Protein motion plays several fundamental roles in protein function, from transmitting the flow of energy and allosteric signals to shuttling a protein via biased routes on the energy landscape for folding and catalysis (Miyashita et al., 2003). The timescales of protein motion span from picosecond to seconds, and the length scales range from local Angstrom motion to nanometer global motion (McCammon, 1984). Understanding nanoscale protein motions is essential, for thermal fluctuations on fast timescales, such as on picosecond to nanosecond timescales, ultimately inspire and dictate the kinetics of large conformational changes necessary for protein function (Bu et al., 2000, 2001, 2005; Lindorff-Larsen et al., 2005; Ishikawa et al., 2008).

The genomic sequence reveals that number of genes, which encode the synthesis of proteins, is far less than the number of proteins in high eukaryotes. In order to make the large number of different proteins that are required to perform diverse cellular functions, one may mix-and-match modular domains in a single polypeptide to make new proteins. As a result, a large number of cellular proteins are multidomain proteins. Protein motions in multidomain proteins, on nanoscales comparable to their overall dimension, are indispensable for relaying signals allosterically in the cellular networks (Ma and Nussinov, 2009). This concept is emerging as a powerful theme in cell signaling. Although we know much about the structure and function of individual modules that compose adapters and scaffolding proteins, their overall dynamic architecture, and in particular the long-range motion properties of scaffolding proteins that control the function of assembled macromolecular signaling complexes, remains a largely unexplored territory.

NHERF1 is a multidomain scaffolding protein that assembles membrane protein clusters, regulate the dynamic trafficking of receptors and ion channels, and organize protein–protein interactions that influence multiple cell signaling pathways. As we proposed in an earlier study, the allosteric regulation of NHERF1 by ezrin to assemble membrane protein complexes could provide a means to effectively control the strength and duration of signaling at the membrane–cytoskeleton (Li et al., 2009). Besides propagating allosteric signals, the long-range “activated” interdomain motions in NHERF1 may serve other functional roles during the assembly of macromolecular complexes. The activated interdomain motion may allow the PDZ domains to sample certain conformational space and to search the target membrane proteins effectively (Windisch et al., 2006).

Using NSE, we have found that the long-range domain motions in the adapter proteins, which are in the nanospatial–temporal regime, relay signals between the F-actin cytoskeletal network and the cell membranes, and exercise control of the assembly of protein complexes in the cell membrane. Our NSE study demonstrates the activation of long-range coupled domain motion on submicrosecond and on nanometer length scales, which influences the long-range allosteric couplings of the different functional domains for binding to target proteins. Remarkably, the changes in protein domain motion are associated with propagating allosteric signals from a binding site to a remote domain that is a distance of 110 Å away.

Protein motion on nanoscales is, at best, difficult to observe by other experimental techniques. The deuterium labeling approach and the theoretical analyses that we presented therefore should pave the way for using NSE to study protein motions in multidomain proteins. We expect NSE to fill an important nanoscale spatial–temporal gap in our ability to characterize protein motion and function.

VI. SUMMARY AND PERSPECTIVE

Allosteric transduction of cellular signals by multiple protein–protein interactions has emerged as an important theme to elucidate the mechanisms of hierarchy signaling pathways and networks. Nanoscale protein domain motions on length scales comparable to protein dimensions hold the key to understanding how signals are relayed through multiple protein–protein interactions. We have explained in this review our view of the present state of protein dynamics, and described our view of the future of this essential field. Protein dynamics (and, in particular, long-range allostery) presents us with a unique paradigm for cell-signaling: the idea that proteins can communicate *within themselves* to effect long-range information transfer. This idea has not been explored, in large part because of a paucity of experimental techniques that can address the necessary questions. We have shown how this burgeoning field can be developed by utilizing NSE spectroscopy to demonstrate long-range coupled protein domain motion. It is essential to recognize the absolute need for interdisciplinary approaches to the study of this very complex problem. For example, one must utilize the concept of a mobility tensor, which in turn is derived from nonequilibrium statistical mechanics, a field which, in itself, is challenging and little explored. We believe that it is impossible not to be excited about the challenges ahead, and the rewards for their successful solution. Nanoscale protein dynamics could hold the key to manipulate protein–protein interactions that comprise the cellular signaling network for therapeutic intervention.

ACKNOWLEDGMENT

This work is supported by National Institutes of Health Grants R01 HL086496.

REFERENCES

- Akcasu, Z., Gurol, H. (1976). Quasi-elastic scattering by dilute polymer-solutions. *J. Polym. Sci., B: Polym. Phys.* **14**, 1–10.
- Bates, I. R., Hébert, B., Luo, Y., Liao, J., Bachir, A. I., Kolin, D. L., et al. (2006). Membrane lateral diffusion and capture of CFTR within transient confinement zones. *Biophys. J.* **91**, 1046–1058.
- Benkovic, S. J., Hammes-Schiffer, S. (2003). A perspective on enzyme catalysis. *Science* **301**, 1196–1202.
- Berne, B. J., Pecora, R. (1976). Dynamic Light Scattering with Applications to Chemistry, Biology and Physics. Dover Publications, Inc., Mineola, New York.
- Bhattacharya, S., Dai, Z., Li, J., Baxter, S., Callaway, D. J. E., Cowburn, D., et al. (2010). A conformational switch in the scaffolding protein NHERF1 controls autoinhibition and complex formation. *J. Biol. Chem.* **285**, 9981–9994.
- Bossard, F., Robay, A., Toumaniantz, G., Dahimene, S., Becq, F., Merot, J., et al. (2007). NHE-RF1 protein rescues ΔF508-CFTR function. *Am. J. Physiol. Lung Cell. Mol. Physiol.* **292**, L1085–L1094.
- Bretscher, A., Chambers, D., Nguyen, R., Reczek, D. (2000). ERM-merlin and EBP50 protein families in plasma membrane organization and function. *Annu. Rev. Cell Dev. Biol.* **16**, 113–143.
- Bretscher, A., Edwards, K., Fehon, R. G. (2002). ERM proteins and merlin: integrators at the cell cortex. *Nat. Rev. Mol. Cell Biol.* **3**, 586–599.
- Bu, Z., Biehl, R., Monkenbusch, M., Richter, D., Callaway, D. J. (2005). Coupled protein domain motion in Taq polymerase revealed by neutron spin-echo spectroscopy. *Proc. Natl. Acad. Sci. USA* **102**, 17646–17651.
- Bu, Z., Cook, J., Callaway, D. J. (2001). Dynamic regimes and correlated structural dynamics in native and denatured alpha-lactalbumin. *J. Mol. Biol.* **312**, 865–873.
- Bu, Z., Engelman, D. M. (1999). A method for determining transmembrane helix association and orientation in detergent micelles using small angle X-ray scattering. *Biophys. J.* **77**, 1064–1073.
- Bu, Z., Neumann, D. A., Lee, S. H., Brown, C. M., Engelman, D. M., Han, C. C. (2000). A view of dynamics changes in the molten globule-native folding step by quasielastic neutron scattering. *J. Mol. Biol.* **301**, 525–536.
- Bu, Z. M., Perlo, A., Johnson, G. E., Olack, G., Engelman, D. M., Wyckoff, H. W. (1998). A small-angle X-ray scattering apparatus for studying biological macromolecules in solution. *J. Appl. Crystallogr.* **31**, 533–543.
- Cao, T. T., Deacon, H. W., Reczek, D., Bretscher, A., von Zastrow, M. (1999). A kinase-regulated PDZ-domain interaction controls endocytic sorting of the beta₂-adrenergic receptor. *Nature* **401**, 286–290.
- Chung, I., Akita, R., Vandlen, R., Toomre, D., Schlessinger, J., Mellman, I. (2010). Spatial control of EGF receptor activation by reversible dimerization on living cells. *Nature* **464**, 783–787.
- Cooper, A., Dryden, D. T. F. (1984). Allostery without conformational change, a plausible model. *Eur. Biophys. J.* **11**, 103–109.

- Creighton, T. E. (1993). Proteins: Structures and Molecular Properties. Freeman and Company, New York.
- Cunningham, R. E. X., Steplock, D., Shenolikar, S., Weinman, E. J. (2005). Defective PTH regulation of sodium-dependent phosphate transport in NHERF-1^{-/-} renal proximal tubule cells and wild-type cells adapted to low-phosphate media. *Am. J. Physiol. Ren. Physiol.* **289**, F933–F938.
- Curto, M., McClatchey, A. I. (2004). Ezrin...a metastatic detERMinant? *Cancer Cell* **5**, 113–114.
- Denker, S. P., Barber, D. L. (2002). Ion transport proteins anchor and regulate the cytoskeleton. *Curr. Opin. Cell Biol.* **14**, 214–220.
- Doi, M., Edwards, S. F. (1986). The Theory of Polymer Dynamics. Oxford University Press, Oxford.
- Donowitz, M., Cha, B., Zachos, N. C., Brett, C. L., Sharma, A., Tse, C. M., et al. (2005). NHERF family and NHE3 regulation. *J. Physiol.* **567**, 3–11.
- Doyle, D. A., Lee, A., Lewis, J., Kim, E., Sheng, M., MacKinnon, R. (1996). Crystal structures of a complexed and peptide-free membrane protein-binding domain: molecular basis of peptide recognition by PDZ. *Cell* **85**, 1067–1076.
- Eisenmesser, E. Z., Millet, O., Labeikovsky, W., Korzhnev, D. M., Wolf-Watz, M., Bosco, D. A., et al. (2005). Intrinsic dynamics of an enzyme underlies catalysis. *Nature* **438**, 117–121.
- Elliott, B. E., Meens, J. A., SenGupta, S. K., Louvard, D., Arpin, M. (2005). The membrane cytoskeletal crosslinker ezrin is required for metastasis of breast carcinoma cells. *Breast Cancer Res.* **7**, R365–R373.
- Farago, B., Li, J., Cornilescu, G., Callaway, D. J., Bu, Z. (2010). Activation of nanoscale allosteric protein domain motion revealed by neutron spin echo spectroscopy. *Biophys. J.* **99**, 3473–3482.
- Favia, M., Guerra, L., Fanelli, T., Cardone, R. A., Monterisi, S., Di Sole, F., et al. (2009). Na⁺/H⁺ exchanger regulatory factor 1 overexpression-dependent increase of cytoskeleton organization is fundamental in the rescue of F508del cystic fibrosis transmembrane conductance regulator in human airway CFBE41o-cells. *Mol. Biol. Cell* **21**, 73–86.
- Fehon, R. (2006). Cell biology: polarity bites. *Nature* **442**, 519–520.
- Fehon, R. G., McClatchey, A. I., Bretscher, A. (2010). Organizing the cell cortex: the role of ERM proteins. *Nat. Rev. Mol. Cell Biol.* **11**, 276–287.
- Ferrand, M., Dianoux, A. J., Petry, W., Zaccâï, G. (1993). Thermal motions and function of bacteriorhodopsin in purple membranes: effects of temperature and hydration studied by neutron scattering. *Proc. Natl. Acad. Sci. USA* **90**, 9668–9672.
- Fersht, A. R. (1998). Structure and Mechanism in Protein Science: a Guide to Enzyme Catalysis and Protein Folding. W.H. Freeman and Company, New York.
- Fievet, B. T., Gautreau, A., Roy, C., Del Maestro, L., Mangeat, P., Louvard, D., et al. (2004). Phosphoinositide binding and phosphorylation act sequentially in the activation mechanism of ezrin. *J. Cell Biol.* **164**, 653–659.
- Fievet, B., Louvard, D., Arpin, M. (2007). ERM proteins in epithelial cell organization and functions. *Biochim. Biophys. Acta Mol. Cell Res.* **1773**, 653–660.

- Fixman, M. (1983). Variational bounds for polymer transport coefficients. *J. Chem. Phys.* **78**, 1588.
- Garbett, D., LaLonde, D. P., Bretscher, A. (2010). The scaffolding protein EBP50 regulates microvillar assembly in a phosphorylation-dependent manner. *J. Cell Biol.* **191**, 397–413.
- Garcia De La Torre, J., Huertas, M. L., Carrasco, B. (2000). Calculation of hydrodynamic properties of globular proteins from their atomic-level structure. *Biophys. J.* **78**, 719–730.
- Gary, R., Bretscher, A. (1995). Ezrin self-association involves binding of an N-terminal domain to a normally masked C-terminal domain that includes the F-actin binding site. *Mol. Biol. Cell* **6**, 1061–1075.
- Gautreau, A., Louvard, D., Arpin, M. (2002). ERM proteins and NF2 tumor suppressor: the Yin and Yang of cortical actin organization and cell growth signaling. *Curr. Opin. Cell Biol.* **14**, 104–109.
- Gerstein, M., Lesk, A. M., Chothia, C. (1994). Structural mechanisms for domain movements in proteins. *Biochemistry* **33**, 6739–6749.
- Gisler, S. M., Stagljar, I., Traebert, M., Bacic, D., Biber, J., Murer, H. (2001). Interaction of the Type IIa Na/Pi cotransporter with PDZ proteins. *J. Biol. Chem.* **276**, 9206–9213.
- Guerra, L., Fanelli, T., Favia, M., Riccardi, S. M., Busco, G., Cardone, R. A., et al. (2005). Na^+/H^+ exchanger regulatory factor isoform 1 overexpression modulates cystic fibrosis transmembrane conductance regulator (CFTR) expression and activity in human airway 16HBE14o-cells and rescues $\Delta\text{F}508$ CFTR functional expression in cystic fibrosis cells. *J. Biol. Chem.* **280**, 40925–40933.
- Haggie, P. M., Kim, J. K., Lukacs, G. L., Verkman, A. S. (2006). Tracking of quantum-dot-labeled CFTR shows immobilization by C-terminal PDZ interactions. *Mol. Biol. Cell* **17**, 4937–4945.
- Haggie, P. M., Stanton, B. A., Verkman, A. S. (2004). Increased diffusional mobility of CFTR at the plasma membrane after deletion of its C-terminal PDZ binding motif. *J. Biol. Chem.* **279**, 5494–5500.
- Hall, R. A., Ostedgaard, L. S., Premont, R. T., Blitzer, J. T., Rahman, N., Welsh, M. J., et al. (1998). A C-terminal motif found in the beta2-adrenergic receptor, P2Y1 receptor and cystic fibrosis transmembrane conductance regulator determines binding to the Na^+/H^+ exchanger regulatory factor family of PDZ proteins. *Proc. Natl. Acad. Sci. USA* **95**, 8496–8501.
- Hall, R. A., Premont, R. T., Chow, C. W., Blitzer, J. T., Pitcher, J. A., Claing, A., et al. (1998). The beta2-adrenergic receptor interacts with the Na^+/H^+ -exchanger regulatory factor to control Na^+/H^+ exchange. *Nature* **392**, 626–630.
- Harris, B. Z., Lim, W. A. (2001). Mechanism and role of PDZ domains in signaling complex assembly. *J. Cell Sci.* **114**, 3219–3231.
- Hawkins, R. J., McLeish, T. C. B. (2004). Coarse-grained model of entropic allostery. *Phys. Rev. Lett.* **93**, 098104.
- Hernando, N., Deliot, N., Gisler, S. M., Lederer, E., Weinman, E. J., Biber, J., et al. (2002). PDZ-domain interactions and apical expression of type IIa Na/P(i) cotransporters. *Proc. Natl. Acad. Sci. USA* **99**, 11957–11962.

- Higgins, J. S., Benoit, H. C. (1994). Polymers and Neutron Scattering. Clarendon Press, Oxford.
- Howard, J. (2001). Mechanics of Motor Proteins and the Cytoskeleton. Sinauer Associates, Sunderland, MA.
- Ishikawa, H., Kwak, K., Chung, J. K., Kim, S., Fayer, M. D. (2008). Direct observation of fast protein conformational switching. *Proc. Natl. Acad. Sci. USA* **105**, 8619–8624.
- James, M. F., Beauchamp, R. L., Manchanda, N., Kazlauskas, A., Ramesh, V. (2004). A NHERF binding site links the betaPDGFR to the cytoskeleton and regulates cell spreading and migration. *J. Cell Sci.* **117**, 2951–2961.
- Karim, Z., Gerard, B., Bakouh, N., Alili, R., Leroy, C., Beck, L., et al. (2008). NHERF1 mutations and responsiveness of renal parathyroid hormone. *N. Engl. J. Med.* **359**, 1128–1135.
- Karthikeyan, S., Leung, T., Birrane, G., Webster, G., Ladias, J. A. (2001). Crystal structure of the PDZ1 domain of human Na(+)/H(+) exchanger regulatory factor provides insights into the mechanism of carboxyl-terminal leucine recognition by class I PDZ domains. *J. Mol. Biol.* **308**, 963–973.
- Karthikeyan, S., Leung, T., Ladias, J. A. (2002). Structural determinants of the Na⁺/H⁺-exchanger regulatory factor interaction with the beta 2 adrenergic and platelet-derived growth factor receptors. *J. Biol. Chem.* **277**, 18973–18978.
- Kerjaschki, D., Sharkey, D. J., Farquhar, M. G. (1984). Identification and characterization of podocalyxin—the major sialoprotein of the renal glomerular epithelial cell. *J. Cell Biol.* **100**, 1591–1596.
- Kern, D., Zuiderweg, E. R. (2003). The role of dynamics in allosteric regulation. *Curr. Opin. Struct. Biol.* **13**, 748–757.
- Khanna, C., Wan, X., Bose, S., Cassaday, R., Olomu, O., Mendoza, A., et al. (2004). The membrane–cytoskeleton linker ezrin is necessary for osteosarcoma metastasis. *Nat. Med.* **10**, 182–186.
- Ko, S. B. H., Zeng, W., Dorwart, M. R., Luo, X., Kim, K. H., Millen, L., et al. (2004). Gating of CFTR by the STAS domain of SLC26 transporters. *Nat. Cell Biol.* **6**, 343–350.
- Kwon, S. H., Pollard, H., Guggino, W. B. (2007). Knockdown of NHERF1 enhances degradation of temperature rescued DeltaF508 CFTR from the cell surface of human airway cells. *Cell. Physiol. Biochem.* **20**, 763–772.
- LaLonde, D. P., Bretscher, A. (2009). The scaffold protein PDZK1 undergoes a head-to-tail intramolecular association that negatively regulates its interaction with EBP50. *Biochemistry* **48**, 2261–2271.
- LaLonde, D. P., Garbett, D., Bretscher, A. (2010). A regulated complex of the scaffolding proteins PDZK1 and EBP50 with ezrin contribute to microvillar organization. *Mol. Biol. Cell* **21**, 1519–1529.
- Lamprecht, G., Seidler, U. (2006). The emerging role of PDZ adapter proteins for regulation of intestinal ion transport. *Am. J. Physiol. Gastrointest. Liver Physiol.* **291**, G766–G777.
- Lazar, C. S., Cresson, C. M., Lauffenburger, D. A., Gill, G. N. (2004). The Na⁺/H⁺-exchanger regulatory factor stabilizes epidermal growth factor receptors at the cell surface. *Mol. Biol. Cell* **15**, 5470–5480.

- Lederer, E. D., Khundmiri, S. J., Weinman, E. J. (2003). Role of NHERF-1 in regulation of the activity of Na-K ATPase and sodium-phosphate co-transport in epithelial cells. *J. Am. Soc. Nephrol.* **14**, 1711–1719.
- Lee, H., Cheng, Y.-C., Fleming, G. R. (2007). Coherence dynamics in photosynthesis: protein protection of excitonic coherence. *Science* **316**, 1462–1465.
- Li, J., Callaway, D. J., Bu, Z. (2009). Ezrin induces long-range interdomain allostery in the scaffolding protein NHERF1. *J. Mol. Biol.* **392**, 166–180.
- Li, J., Dai, Z., Jana, D., Callaway, D. J., Bu, Z. (2005). Ezrin controls the macromolecular complexes formed between an adapter protein Na^+/H^+ exchanger regulatory factor and the cystic fibrosis transmembrane conductance regulator. *J. Biol. Chem.* **280**, 37634–37643.
- Li, Q., Nance, M. R., Kulikauskas, R., Nyberg, K., Fehon, R., Karplus, P. A., et al. (2007). Self-masking in an intact ERM-merlin protein: an active role for the central alpha-helical domain. *J. Mol. Biol.* **365**, 1446–1459.
- Li, J., Poulikakos, P. I., Dai, Z., Testa, J. R., Callaway, D. J., Bu, Z. (2007). Protein kinase C phosphorylation disrupts Na^+/H^+ exchanger regulatory factor 1 autoinhibition and promotes cystic fibrosis transmembrane conductance regulator macromolecular assembly. *J. Biol. Chem.* **282**, 27086–27099.
- Lindorff-Larsen, K., Best, R. B., Depristo, M. A., Dobson, C. M., Vendruscolo, M. (2005). Simultaneous determination of protein structure and dynamics. *Nature* **433**, 128–132.
- Liu, Y., Belkina, N. V., Shaw, S. (2009). HIV infection of T cells: actin-in and actin-out. *Science* **2pe23**.
- Liu-Chen, L. Y. (2004). Agonist-induced regulation and trafficking of kappa opioid receptors. *Life Sci.* **75**, 511–536.
- Ma, B., Nussinov, R. (2009). Amplification of signaling via cellular allosteric relay and protein disorder. *Proc. Natl. Acad. Sci. USA* **106**, 6887–6888, Epub 2009 Apr 6822.
- Mahon, M. J. (2008). Ezrin promotes functional expression and parathyroid hormone-mediated regulation of the sodium-phosphate cotransporter 2a in LLC-PK1 cells. *Am. J. Physiol. Ren. Physiol.* **294**, F667–F675.
- Mahon, M. J., Donowitz, M., Yun, C. C., Segre, G. V. (2002). $\text{Na}(+)/\text{H}(+)$ exchanger regulatory factor 2 directs parathyroid hormone 1 receptor signalling. *Nature* **417**, 858–861.
- Mahon, M. J., Segre, G. V. (2004). Stimulation by parathyroid hormone of a NHERF-1-assembled complex consisting of the parathyroid hormone I receptor, phospholipase C β , and actin increases intracellular calcium in opossum kidney cells. *J. Biol. Chem.* **279**, 23550–23558.
- Mangia, A., Chiriatti, A., Bellizzi, A., Malfettone, A., Stea, B., Zito, F. A., et al. (2009). Biological role of NHERF1 protein expression in breast cancer. *Histopathology* **55**, 600–608.
- Matsui, T., Maeda, M., Doi, Y., Yonemura, S., Amano, M., Kaibuchi, K., et al. (1998). Rho-kinase phosphorylates COOH-terminal threonines of ezrin/radixin/moesin (ERM) proteins and regulates their head-to-tail association. *J. Cell Biol.* **140**, 647–657.
- Matsui, T., Yonemura, S., Tsukita, S. (1999). Activation of ERM proteins *in vivo* by Rho involves phosphatidyl-inositol 4-phosphate 5-kinase and not ROCK kinases. *Curr. Biol.* **9**, 1259–1262.

- Maudsley, S., Zamah, A. M., Rahman, N., Blitzer, J. T., Luttrell, L. M., Lefkowitz, R. J., et al. (2000). Platelet-derived growth factor receptor association with Na(+)/H(+) exchanger regulatory factor potentiates receptor activity. *Mol. Cell. Biol.* **20**, 8352–8363.
- McCammon, J. A. (1984). Protein dynamics. *Rep. Prog. Phys.* **47**, 1–46.
- McClatchey, A. I. (2003). Merlin and ERM proteins: unappreciated roles in cancer development? *Nat. Rev. Cancer* **3**, 877–883.
- McClatchey, A. I., Fehon, R. G. (2009). Merlin and the ERM proteins—regulators of receptor distribution and signaling at the cell cortex. *Trends Cell Biol.* **19**, 198–206, Epub 2009 Apr 2001.
- Mezei, F. (1980). The Principles of Neutron Spin Echo, Neutron Spin Echo: Proceedings of a Laue-Langevin Institut Workshop. Springer, Heidelberg.
- Mi, H., Endo, T., Schreiber, U., Ogawa, T., Asada, K. (1994). NAD(P)H dehydrogenase-dependent cyclic electron flow around photosystem I in the *Cyanobacterium synechocystis* PCC 6803: a study of dark-starved cells and spheroplasts. *Plant Cell Physiol.* **35**, 163–173.
- Miyashita, O., Onuchic, J. N., Wolynes, P. G. (2003). Nonlinear elasticity, protein-quakes, and the energy landscapes of functional transitions in proteins. *Proc. Natl. Acad. Sci. USA* **100**, 12570–12575.
- Morales, F. C., Takahashi, Y., Momin, S., Adams, H., Chen, X., Georgescu, M. M. (2007). NHERF1/EBP50 head-to-tail intramolecular interaction masks association with PDZ domain ligands. *Mol. Cell. Biol.* **27**, 2527–2537.
- Moyer, B. D., Duhaime, M., Shaw, C., Denton, J., Reynolds, D., Karlson, K. H., et al. (2000). The PDZ-interacting domain of cystic fibrosis transmembrane conductance regulator is required for functional expression in the apical plasma membrane. *J. Biol. Chem.* **275**, 27069–27074.
- Naren, A. P., Cobb, B., Li, C., Roy, K., Nelson, D., Heda, G. D., et al. (2003). A macromolecular complex of beta 2 adrenergic receptor, CFTR, and ezrin/radixin/moesin-binding phosphoprotein 50 is regulated by PKA. *Proc. Natl. Acad. Sci. USA* **100**, 342–346.
- Palmer, A. G., 3rd. (2004). NMR characterization of the dynamics of biomacromolecules. *Chem. Rev.* **104**, 3623–3640.
- Perez-Moreno, M., Jamora, C., Fuchs, E. (2003). Sticky business: orchestrating cellular signals at adherens junctions. *Cell* **112**, 535–548.
- Petoukhov, M. V., Svergun, D. I. (2006). Joint use of small-angle X-ray and neutron scattering to study biological macromolecules in solution. *Eur. Biophys. J.* **35**, 567–576.
- Pettersen, E. F., Goddard, T. D., Huang, C. C., Couch, G. S., Greenblatt, D. M., Meng, E. C., et al. (2004). UCSF chimera—a visualization system for exploratory research and analysis. *J. Comput. Chem.* **25**, 1605–1612.
- Pollard, T. D., Cooper, J. A. (2009). Actin, a central player in cell shape and movement. *Science* **326**, 1208–1212.
- Prat, A. G., Cunningham, C. C., Jackson, G. R., Jr., Borkan, S. C., Wang, Y., Ausiello, D. A., et al. (1999). Actin filament organization is required for proper cAMP-dependent activation of CFTR. *Am. J. Physiol.* **277**, C1160–C1169.

- Pujuguet, P., Del Maestro, L., Gautreau, A., Louvard, D., Arpin, M. (2003). Ezrin regulates Ecadherin-dependent adherens junction assembly through Rac1 activation. *Mol. Biol. Cell* **14**, 2181–2191, Epub 2003 Feb 2186.
- Raghuram, V., Mak, D. D., Foskett, J. K. (2001). Regulation of cystic fibrosis transmembrane conductance regulator single-channel gating by bivalent PDZ-domain-mediated interaction. *Proc. Natl. Acad. Sci. USA* **98**, 1300–1305.
- Reczek, D., Berryman, M., Bretscher, A. (1997). Identification of EBP50: a PDZ-containing phosphoprotein that associates with members of the ezrin–radixin–moesin family. *J. Cell Biol.* **139**, 169–179.
- Reczek, D., Bretscher, A. (1998). The carboxyl-terminal region of EBP50 binds to a site in the amino-terminal domain of ezrin that is masked in the dormant molecule. *J. Biol. Chem.* **273**, 18452–18458.
- Roch, F., Polesello, C., Roubinet, C., Martin, M., Roy, C., Valenti, P., et al. (2010). Differential roles of PtdIns(4,5)P₂ and phosphorylation in moesin activation during *Drosophila* development. *J. Cell Sci.* **123**, 2058–2067.
- Roumier, A., Olivo-Marin, J. C., Arpin, M., Michel, F., Martin, M., Mangeat, P., et al. (2001). The membrane-microfilament linker ezrin is involved in the formation of the immunological synapse and in T Cell activation. *Immunity* **15**, 715–728.
- Schlessinger, J. (1988). Signal transduction by allosteric receptor oligomerization. *Trends Biochem. Sci.* **13**, 443–447.
- Schmieder, S., Nagai, M., Orlando, R. A., Takeda, T., Farquhar, M. G. (2004). Podocalyxin activates RhoA and induces actin reorganization through NHERF1 and ezrin in MDCK cells. *J. Am. Soc. Nephrol.* **15**(9), 2289–2298.
- Scott, J. D., Pawson, T. (2009). Cell signaling in space and time: where proteins come together and when they're apart. *Science* **326**, 1220–1224.
- Sheng, M., Sala, C. (2001). PDZ domains and the organization of supramolecular complexes. *Annu. Rev. Neurosci.* **24**, 1–29.
- Shenolikar, S., Voltz, J. W., Cunningham, R., Weinman, E. J. (2004). Regulation of ion transport by the NHERF family of PDZ proteins. *Physiology (Bethesda)* **19**, 362–369.
- Short, D. B., Trotter, K. W., Reczek, D., Kreda, S. M., Bretscher, A., Boucher, R. C., et al. (1998). An apical PDZ protein anchors the cystic fibrosis transmembrane conductance regulator to the cytoskeleton. *J. Biol. Chem.* **273**, 19797–19801.
- Singh, A. K., Riederer, B., Krabbenhöft, A., Rausch, B., Bonhagen, J., Lehmann, U., et al. (2009). Differential roles of NHERF1, NHERF2, and PDZK1 in regulating CFTR-mediated intestinal anion secretion in mice. *J. Clin. Investig.* **119**, 540–550.
- Sizemore, S., Cicek, M., Sizemore, N., Ng, K. P., Casey, G. (2007). Podocalyxin increases the aggressive phenotype of breast and prostate cancer cells *in vitro* through its interaction with ezrin. *Cancer Res.* **67**, 6183–6191.
- Sneddon, W. B., Syme, C. A., Bisello, A., Magyar, C. E., Rochdi, M. D., Parent, J. L., et al. (2003). Activation-independent parathyroid hormone receptor internalization is regulated by NHERF1 (EBP50). *J. Biol. Chem.* **278**, 43787–43796.
- Somasiri, A., Nielsen, J. S., Makretsov, N., McCoy, M. L., Prentice, L., Gilks, C. B., et al. (2004). Overexpression of the anti-adhesin podocalyxin is an independent predictor of breast cancer progression. *Cancer Res.* **64**(15), 5068–5073.

- Svergun, D. I. (1999). Restoring low resolution structure of biological macromolecules from solution scattering using simulated annealing. *Biophys. J.* **76**, 2879–2886.
- Takahashi, Y., Morales, F. C., Kreimann, E. L., Georgescu, M. M. (2006). PTEN tumor suppressor associates with NHERF proteins to attenuate PDGF receptor signaling. *EMBO J.* **25**, 910–920.
- Takeda, T., McQuistan, T., Orlando, R. A., Farquhar, M. G. (2001). Loss of glomerular foot processes is associated with uncoupling of podocalyxin from the actin cytoskeleton. *J. Clin. Invest.* **108**, 289–301.
- Taouil, K., Hinnrasky, J., Hologne, C., Corlieu, P., Klossek, J. M., Puchelle, E. (2003). Stimulation of beta 2-adrenergic receptor increases cystic fibrosis transmembrane conductance regulator expression in human airway epithelial cells through a cAMP/protein kinase A-independent pathway. *J. Biol. Chem.* **278**, 17320–17327.
- Terawaki, S.-i., Maesaki, R., Hakoshima, T. (2006). Structural basis for NHERF recognition by ERM proteins. *Structure* **14**, 777–789.
- Thelin, W. R., Hodson, C. A., Milgram, S. L. (2005). Beyond the brush border: NHERF4 blazes new NHERF turf. *J. Physiol.* **567**, 13–19.
- Verpy, E., Leibovici, M., Zwaenepoel, I., Liu, X. Z., Gal, A., Salem, N., et al. (2000). A defect in harmonin, a PDZ domain-containing protein expressed in the inner ear sensory hair cells, underlies Usher syndrome type 1C. *Nat. Genet.* **26**, 51–55.
- Wang, C., Pan, L., Chen, J., Zhang, M. (2010). Extensions of PDZ domains as important structural and functional elements. *Protein Cell* **1**, 737–751.
- Weinman, E. J., Hall, R. A., Friedman, P. A., Liu-Chen, L. Y., Shenolikar, S. (2006). The association of NHERF adaptor proteins with g protein-coupled receptors and receptor tyrosine kinases. *Annu. Rev. Physiol.* **68**, 491–505.
- Weinman, E. J., Wang, Y., Wang, F., Greer, C., Steplock, D., Shenolikar, S. (2003). A C-terminal PDZ motif in NHE3 binds NHERF-1 and enhances cAMP inhibition of sodium-hydrogen exchange. *Biochemistry* **42**, 12662–12668.
- Windisch, B., Bray, D., Duke, T. (2006). Balls and chains—a mesoscopic approach to tethered protein domains. *Biophys. J.* **91**, 2383–2392.
- Wong, W., Gough, N. R. (2009). Focus issue: the protein dynamics of cell signaling. *Sci. STKE* **2**, eg4.
- Yao, S., Babon, J. J., Norton, R. S. (2008). Protein effective rotational correlation times from translational self-diffusion coefficients measured by PFG-NMR. *Biophys. Chem.* **136**, 145–151.
- Yap, A. S., Brieher, W. M., Gumbiner, B. M. (1997). Molecular and functional analysis of cadherin-based adherens junctions. *Annu. Rev. Cell Dev. Biol.* **13**, 119–146.
- Yonemura, S., Matsui, T., Tsukita, S. (2002). Rho-dependent and -independent activation mechanisms of ezrin/radixin/moesin proteins: an essential role for polyphosphoinositides *in vivo*. *J. Cell Sci.* **115**, 2569–2580.
- Yu, Y., Khan, J., Khanna, C., Helman, L., Meltzer, P. S., Merlino, G. (2004). Expression profiling identifies the cytoskeletal organizer ezrin and the developmental homeoprotein Six-1 as key metastatic regulators. *Nat. Med.* **10**, 175–181.
- Zaccai, G. (2000). How soft is a protein? A protein dynamics force constant measured by neutron scattering. *Science* **288**, 1604–1607.

